A Jacking Force Study Based on Interpretation of Box Jacking Records: A Case Study of Curved Rectangular Box Jacking in Soft Soil in Saitama, Japan

Yu, Bosong
Labotatory of Rock Engineering and Mining Machinery, Department of Earth Resources Engineering, Kyushu University

Shimada, Hideki
Labotatory of Rock Engineering and Mining Machinery, Department of Earth Resources Engineering, Kyushu University

Sasaoka, Takashi
Labotatory of Rock Engineering and Mining Machinery, Department of Earth Resources Engineering, Kyushu University

Hamanaka, Akihiro
Labotatory of Rock Engineering and Mining Machinery, Department of Earth Resources Engineering, Kyushu University

他

https://hdl.handle.net/2324/6788775

出版情報：Tunnelling and Underground Space Technology. 139, pp.105228-, 2023-05-26. Elsevier
バージョン：

A Jacking Force Study Based on Interpretation of Box Jacking Records: A Case Study of Curved Rectangular Box Jacking in Soft Soil in Saitama, Japan

Bosong Yu[1], Hideki Shimada[1,2], Takashi Sasaoka[1], Akihiro Hamanaka[1]*, Fumihiko Matsumoto[2], Tomo Morita[2]

[1]Labotatory of Rock Engineering and Mining Machinery, Department of Earth Resources Engineering, Kyushu University, Fukuoka 819-0395, Japan

[2]Alpha Civil Engineering, Fukuoka 812-0015, Japan

*Corresponding author.

E-mail address: hamanaka@mine.kyushu-u.ac.jp (Akihiro Hamanaka)

Telephone number: +81-092-802-3331 (Akihiro Hamanaka)

Abstract: Box-jacking as a tunnelling method has gained popularity in recent years for locating underground utilities and infrastructure. Nevertheless, the employment of this technique still poses challenges, particularly in predicting the jacking force of long drives. Accurate prediction of jacking force is highly desirable for anomaly detection, avoiding thrust overload limits, and protecting the box culverts and launch shafts from damage. However, such a prediction entails accounting for numerous factors, including site geology, lubricated overcut, work stoppages, deviations in alignment, and the driving style of the tunnel boring machine. In this paper, technical details of a Japan box-jacking project totalling over 220 m in length are discussed, with a focus on elucidating the relationship between tunnelling parameters and jacking force. Then, calculating approaches for forecasting jacking force during curved box-jacking are introduced. The modified Box-soil-lubricant contact model based on the analysis of tunnelling parameters is adopted for this purpose which can improve the accuracy of forecasts. Forecasts determined by the proposed approach are appraised through comparisons to predictions obtained using the PBK method currently utilized in industry. The results show that the proposed approach provides better forecasts of the monitored field data and highlight the significance of interpreting field data as a valuable tool for assimilating the experience with box-jacking in various ground conditions.

Key words Box-jacking; Frictional resistance; Stoppages; Box-soil-lubricant interaction; Calculation model.

Acknowledgements

This research was made possible by financial support from the China Scholarship Council (CSC). The authors wish to express their gratitude to Alpha Civil Engineering Co., Ltd. in Fukuoka, Japan, for providing the necessary machine information and for their valuable contributions to the TBM data analysis and performance through insightful comments and fruitful discussions

Declaration of Competing Interest

The author declares that there is no conflict of interest.

CRediT authorship contribution statement

Bosong Yu: Conceptualization, Methodology, Investigation, Writing – original draft, Writing – review & editing, Formal analysis, Visualization. **Hideki Shimada**: Conceptualization, Supervision, Project administration, Funding acquisition. **Takashi Sasaoka**: Investigation, Supervision, Funding acquisition. **Akihiro Hamanaka**: Supervision. **Fumihiko Matsumoto**: Investigation, Resources, Project administration. **Tomo Morita:** Investigation, Resources, Project administration.

A Jacking Force Study Based on Interpretation of Box Jacking Records: A Case Study of Curved Rectangular Box Jacking in Soft Soil in Saitama, Japan

Abstract: Box-jacking as a tunnelling method has gained popularity in recent years for locating underground utilities and infrastructure. Nevertheless, the employment of this technique still poses challenges, particularly in predicting the jacking force of long drives. Accurate prediction of jacking force is highly desirable for anomaly detection, avoiding thrust overload limits, and protecting the box culverts and launch shafts from damage. However, such a prediction entails accounting for numerous factors, including site geology, lubricated overcut, work stoppages, deviations in alignment, and the driving style of the tunnel boring machine. In this paper, technical details of a Japan box-jacking project totalling over 220 m in length are discussed, with a focus on elucidating the relationship between tunnelling parameters and jacking force. Then, calculating approaches for forecasting jacking force during curved box-jacking are introduced. The modified Box-soil-lubricant contact model based on the analysis of tunnelling parameters is adopted for this purpose which can improve the accuracy of forecasts. Forecasts determined by the proposed approach are appraised through comparisons to predictions obtained using the PBK method currently utilized in industry. The results show that the proposed approach provides better forecasts of the monitored field data and highlight the significance of interpreting field data as a valuable tool for assimilating the experience with box-jacking in various ground conditions.

Key words Box-jacking; Frictional resistance; Stoppages; Box-soil-lubricant interaction; Calculation model.

1. Introduction

In recent times, the use of trenchless method in constructing utility tunnels and underground infrastructure has seen a significant increase in response to the rapidly growing demand for urbanization, renewable energy, and economic development in emerging regions. Rectangular box-jacking is a commonly utilized trenchless technology for constructing underground pedestrian passageways, subways, and utility tunnels, including those for sewer, stormwater, fiber optics, and electricity pipelines. The use of this method presents several benefits, such as high space utilization, cost-effectiveness, short construction duration, and strong adaptability for shallow overburden tunnels (Chen et al., 2021; Li, 2017; Luo et al., 2020; Sterling, 2020; Valdenebro and Gimena, 2018). Moreover, the box-jacking method causes less disturbance to urban areas compared to conventional techniques such as cut and cover (Curran, 2011; Kaushal et al., 2020; Lu et al., 2020; Tavakoli et al., 2017).

The box-jacking technology operates by using powerful hydraulic jacks to advance a Tunnel Boring Machine (TBM) and prefabricated box culverts from a launch shaft into the ground, with the TBM excavating the soil as it moves towards a receiving shaft. (Milligan and Norris, 1996; Pellet-Beaucour and Kastner, 2002). With growing complexity of construction requirements, the construction distances have increased over the years (Chen et al., 2021). To accommodate long-distance construction, intermediate jacking shafts are usually required. However, these shafts significantly raise costs and cause construction delays. Therefore, long-drive box jacking, often with curves, is desirable in the industry to avoid the need for intermediate shafts and their associated expenses (Bergeson, 2014). For safety, the jacking force applied to the box culverts during the jacking construction must be limited to the maximum permissible compressive strength, which determines the maximum jacking force (Namli and Guler, 2017). In this situation, one of the biggest risks in long-drive box jacking is the buildup of excessive soil-structure penetration resistance, which can exceed the total available jacking force. The total jacking force in long-drive box jacking is mostly determined by frictional resistance between the soil and structure (Cheng et al., 2017). Therefore, accurately predicting the frictional resistance is crucial in preventing damage to the box.

Currently, site engineers typically combine empiricism from on-site experience with ad hoc theoretical relationships to estimate the frictional resistance (Sheil, 2021). However, the accuracy of the frictional resistance prediction is affected by various factors, including geology of jacking site, lubricating effect, curved jacking section, stoppages and pipe misalignment (Cheng et al., 2017; Meskele and Stuedlein, 2015; Sun et al., 2019). The interaction between pipe, lubricant and soil is governed by the combined effect of overcutting and lubricating, which have a bearing on the development of frictional resistance. (Shou et al., 2010). Furthermore, the performance of the lubricant also has an effect on the friction force (Maehara et al., 2019; Reilly and Orr, 2017; Shou et al., 2010). According to field studies, the use of lubricants can reduce skin friction by up to 90% (Reilly and Orr, 2017).

In addition to conventional linear jacking project, the use of curved jacking technique has become increasingly common in the last two decades. Compared with linear jacking, friction prediction of curved jacking is more complex and requires consideration of additional friction on the outside of curve due to the lateral jacking force (Beckmann et al., 2007; Nanno, 1996). Meanwhile, stoppages during jacking process result in localized spikes in the required jacking force due to the increase in soil-structure penetration resistance (Chapman and Ichioka, 1999; Cheng et al., 2017; Zhang et al., 2018). These spikes typically dictate the jacking force requirements. Several authors have quantified the rise in jacking force after stoppages, but their findings are not entirely uniform (Cheng et al., 2018; Curran, 2011; Reilly and Orr, 2012; Zhang et al., 2018). Hence, there is still a need for further research on the impact of stoppages on jacking forces.

This paper aims to ascertain the methodologies for assessing the box-lubricant-soil contact status, as well as calculating the frictional resistance. To attain the aforementioned objective, tunnelling data gathered from a Japan box-jacking monitoring project undergoes analysis to provide insight into several of the knowledge gaps identified above.

2. Box jacking project and tunnelling details

2.1 Project Overview

The Ougi-dori line stormwater trunk project in the Nishi-Omiya area was designed to solve the drainage issues along the Ougi-dori line and mitigate the risk of flooding during the rainy season. The project was located between two schools that experience a lot of congestion during rush hour. To minimize the impact on traffic, the rectangular box jacking method was selected to construct a tunnel with 3.3 m by 2.5 m rectangular box culverts. The tunnel was constructed by Tobishima Construction Ltd. The location of tunnel and shafts is illustrated in **Fig. 1**.

2.2 Drive details

The total length of this partially curved tunnel was 220.97 m, and its route is depicted in **Fig. 2**. It included two circular curves with radii of curvature of 100 m and lengths of 45.09 m and 64.87 m, respectively. The cover depth in this project ranged from 0.97 m to 3.91 m, which is shallow and exhibits significant variation. The Earth Pressure Balance (EPB) pipe-jacking machine with multi-axis rotation cutting method used in this project was developed by Alpha Civil Engineering Ltd. The cutterhead had an outer dimension of 3370 mm in width and 2570 mm in height, and it was equipped with four earth pressure sensors to monitor the earth pressure acting on its face. As typical for rectangular box jacking projects, the pipe jacking machine was equipped with one revolution cutterhead and three rotation cutterhead. The EPB pipe-jacking machine had a maximal revolution of 1.28 rev/min and a maximal torque of 1091.5 kNm for the revolution cutterhead. For the rotational cutterhead driven by the revolution axis, it had a maximal revolution of 5.12 rev/min and a maximal torque of 272.9 kNm. The cutterhead with dimension parameters is illustrated in **Fig. 3** and some important machine specifications are summarized in **Table 1**. The operator can control the rotational frequency of the EPB pipe-jacking machine's revolution by adjusting the input current. By varying the rotational frequency, the torque and cutting force of the cutter bits can be further managed.

To improve the followability of the box culverts, ten shield jacks were set to control the direction which can be seen in **Fig. 3**(c). These shield jacks can also be used as a backup device to propel the cutterhead when it encounters obstacles such as pebbles and woodpiles, without relying on the pressure of the main jack in the launch shaft. The construction period lasted nearly 3 months, for a total of 57 working days. During this period, there were several long shutdowns, including the new year holiday in Japan, which lasted up to 5 days. Each concrete box culvert was 1.25 m long with outside dimensions of 2500 mm high and 3300 mm width, providing an overcut 35 mm thick. The mass of each box culvert was about 10 500 kg. **Fig. 4** shows the structure and field scene diagram of box culvert diagrammatically.

2.3 Geological conditions at the study site

According to the geological survey, shallow stratum of the Nishi-Omiya, where the Ougi-dori project was located, was almost dominated by soft soils. This project included four boreholes: BH1, BH2, BH3, and BH4. BH4 was not located within the jacking route and its main purpose is to reveal the ground conditions near the reception shaft. The locations of these boreholes in relation to the jacking route are shown in **Fig. 1**. Through these geological boreholes, various soils were discovered, including made ground, underlain by sandy silt/silt, peat, and silty sand/sand. Based on the stratigraphic summary presented in **Fig. 5**, it was observed that the box string traversed through the soft silt layers, followed by the silty sand formations, and finally may have entered the made ground. Meanwhile, the geological boreholes also show that the water table ranged from the depth of 9.5 m to 10.3 m.

Uncorrected Standard Penetration Test (SPT) values N are also shown in **Fig. 5**. The SPT N value can objectively determine the softness, hardness, and compactness of the soil. Through the accumulation of data and regression analysis, it is possible to infer the physical parameters of the soil (Stroud, 1989). In order to derive the earth pressure acting on the box for jacking force prediction, the average N_a values for every layer were used to obtain the physical parameters of soil (Matsumoto, 1998), as shown in **Table 2**.

2.4 Details of lubricant technology

In the Ougi-dori project, which involves long drive box jacking under complex geological conditions, it is necessary to use lubricant to reduce the skin friction between the soil and pipe train (Shou et al., 2010). The box culverts were jacked below the groundwater table, so a two-component consolidated lubricant was used to prevent groundwater intrusion and provide an anti-friction effect.

In Japan, two-component consolidated lubricant is a commonly used lubricant for pipe jacking projects. It consists of A-component, which contains sodium silicate polymer and B-component, which contains a mixture of food additives and high-purity montmorillonite (Ma et al., 2022). Upon mixing A-component with B-component for a period, the lubricant solidifies, as shown in **Fig. 6**. The solidification time decreases with an increase in the amount of A-component added and may range from 10-60 seconds. For the standard formulation used in this project, the solidification time is approximately 30 seconds. The Standard formulation for this lubricant is shown in **Table 3**. By comparing the size of outer profile of the pipe jacking machine and box culvert, t=35 mm overcut was generated on the outside of box culverts. While considering the fluid filling on the excavation face and soil deformation, only the 17.5mm of overcut was used to calculate the lubrication volume (JSTT, 2018). Given that the project mainly passed through silty and silty sand layers that are susceptible to lubricant leakage and contained high levels of groundwater, the grouting volume was designed to be twice the theoretical grouting volume calculated based on theoretical overcutting. The surplus lubricant seeped into the ground and formed a complete filter cake, which provided an adequate anti-friction effect.

Fig. 4 presents a schematic diagram of the layout of lubricant injection holes. The diameter of the grouting holes was 50 mm, and each hole was set on one of the four walls. The grouting holes of the top and bottom slab were 900 mm away from the closer side wall. For this project, the injection pressure was controlled around 0.1 MPa.

3. Monitoring results and analysis

During the whole drive, the average output data from box jacking machine was recorded at intervals of 30 seconds, including local time, jacked distance, total jacking force, current of cutterhead and face pressure. To better represent in graphics, the data was averaged for each box culvert (about 1.25 m). Because of some technical issues with data collection system, data of eight box culverts totaling ten meters in three days of November 7th, 18th and December 21st were lost. The overall regularity of the data is good, so the impact of a small amount of data loss is negligible.

3.1 Jacking force

In box jacking construction, the total jacking force (F_{total}) can be divided into two parts: force (F_{face}) acting on the face of the TBM, and the frictional resistance ($F_{friction}$) between structure (including TBM and box string) and the surrounding soil.

3.1.1 Face resistance

As stated in Section 2.2, the face resistance (F_{face}) was recorded by the earth pressure sensors arranged on the chamber wall of the TBM. F_{face} was calculated by averaged earth pressure (P_{face}), as shown in Eq. (1):

$$F_{face} = P_{face} \times B \times H \quad (1)$$

F_{face} with jacked distance is demonstrated in **Fig. 7**, with the cover depth curve obtained by connecting the elevation measured at each measuring point (BC1, EC1, BC2, EC2). The highest F_{face} of approximately 900 kN was experienced at a jacked distance of about 140 m with a cover depth of over 2 m, which then steadily decreased to less than 500 kN as TBM approached the reception shaft (the overlaying soil near the reception shaft was getting shallower, and the shallowest point was only 0.97 m).

Despite a slight reduction in cover depth, F_{face} displays a slight increasing trend after a jacked distance of approximately 75 m, as illustrated in **Fig. 7**. This increase could be due to the change in stratum during jacking process. The change in stratum can be deduced from the variations in cutterhead current and penetration rate, which are presented in **Fig. 8**. Beyond a jacked length of 75 m, the average value of cutterhead current rose from 65 A to 75 A, indicating that the torque required to cut the soil also increased. The cutterhead current did not drop back to 65 A, until the total jacked distance reached 190 m. Therefore, it can be deduced that the soil between 75 and 190 m was harder. Geological borehole data corroborates this deduction that the TBM primarily drove through silty sand from BH2 to BH3, as depicted in **Fig. 5**. The opposite trend of penetration rate, as shown in **Fig. 8**, also supports this conclusion. TBM operators tend to lower the penetration rate when TBM is driving through harder strata (Cheng et al., 2017; Lehmann et al., 2022). At the beginning of the drive, the averaged penetration rate was 47.6 mm/min in the silt. After a jacked length of 75 m, the penetration rate decreased to an average of 37.9 mm/min in the silty sand. When the TBM entered the soft stratum again around 190 m, the penetration rate was re-adjusted to 43.3 mm/min, accompanied by a significant decrease in F_{face} shown in **Fig. 7**. Furthermore, the time required to jack each box also serves as an indicator of changes in the stratum. As illustrated in **Fig. 9**, when the TBM encountered silty sand, the average construction time increased by approximately 20 minutes. According to above analysis, the stratum traversed by TBM can be roughly divided into three categories as shown in **Fig. 8**: silt (0-75 m), silty sand (75-190 m), and made ground (190 m to the reception shaft).

It should be noted that as the TBM approached the reception shaft, there was a significant reduction in the penetration rate. The most likely explanation for this phenomenon is the various inspections that were conducted before the final completion of the construction. Throughout this period, the implementation of frequent daily checks was found to have a significant impact on construction time. Specifically, the time required for installing single box increased from approximately one hour to over two hours, leading to a reduction in the penetration rate, as illustrated in **Fig. 9**.

3.1.2 Frictional resistance

For long-drive jacking, $F_{friction}$ is often the main contribution to the F_{total} (Cheng et al., 2017). According to the total jacking force composition, $F_{friction}$ can be obtained by subtracting the F_{face} from the F_{total}. The development of the $F_{friction}$ with jacked distance is shown in **Fig. 10**. The trend overall indicated an increase in $F_{friction}$ with jacked length, albeit with variations in the rate of increase observed across different stages. The averaged friction resistance gradient with jacked distance was derived by analyzing the overall trend of $F_{friction}$ across different stages, as illustrated in **Fig. 11**. Notably, the increase rate of $F_{friction}$ was found to decline beyond a jacked distance of 75 m. The observed phenomenon can be attributed to a combination of factors, including the TBM's crossing of relatively harder strata and the accumulation of lubricant in overcutting area.

The crossing stratum in this project consists of soft soils such as silt and made ground, as well as medium-dense silty sand which is relatively harder. Hashimoto and Brinkman reported the variation model of lining pressure with injection pressure for different stratum as shown in **Fig. 12** (T. Hashimoto, 2004). In soft soil, the lubricant pressure gradually dissipates, and the lateral soil (soil along the sides of box culverts) eventually collapse on the box wall. By contrast, when driving in the hard soil which has a certain self-supporting capacity, the lateral soil hardly deforms laterally. Hence, when TBM was navigating through silt before a jacked distance of 75 m in this project, both sides of box culvert may have come into contact with the surrounding soil through the lubricant and bore the active earth pressure. However, after encountering silty sand, this contact was altered to box-lubricant contact, which greatly reduces the friction coefficient between box and soil.

Another possible reason for the decrease in the increase rate of $F_{friction}$ after 75 m may be the accumulation of lubricant. As shown in **Fig. 10**, the volume of lubricant gradually increased with the increase in jacking distance, and the effectiveness of the lubricant became more apparent. This obvious lubricant effect on $F_{friction}$ is also evident in the studies conducted by other researchers (Cheng et al., 2017; Ji et al., 2019a; O'Dwyer et al., 2020; Zhang et al., 2022). In the reported projects, the volume of injected lubricant exceeded the theoretical overcut annulus significantly, with a typical volume ratio of 2-4 and a maximum ratio of 6.66. The effectiveness of lubricant can be assessed by skin friction (τ) values (O'Dwyer et al., 2020). It can be seen from **Fig. 13** that the skin friction value at the beginning of the drive was very high due to the combination of a heavy non-lubricated TBM shield likely dragging along the bottom of the overcut and the relatively short tunnel length. However, as drive length increased, these effects became negligible, and the skin friction value significantly decreased. According to Praetorius and Schößer (2017), the average skin friction of the Ougi-dori project before 75 m can be considered "Very poor" at 5.20 kPa, when not considering the influence of the originating segment. This suggests that within this section of the project, more than one side of the box was in contact with the surrounding soil. **Fig. 13** shows that the skin friction remained consistently low after a jacked distance of 75 m. This phenomenon reveals the improved lubricating effect, which is consistent with the observed drop about 1000 kN in $F_{friction}$ and a negative rate of change in $F_{friction}$, as shown in **Fig. 10** and **Fig. 11**, respectively. The improved lubrication may lead to a decrease in the box-soil contact area, which in turn causes a reduction in the friction resistance gradient. This reduction contributes to a decrease of approximately 23 kN/m in the increase rate of $F_{friction}$ as TBM navigated in silty sand, as depicted in **Fig. 11**.

Furthermore, it is worth noting that the skin friction did not drop to 2.86 kPa immediately after a jacked length of 75 m, but rather to a higher value of 4.20 kPa between 75-100 m. This corresponds to the abnormal change in $F_{friction}$ (**Fig. 10**) within this chainage interval, which could be due to a technical issue with the box culvert connection. During this period, due to uneven shrinkage of the sealing rubber, water leakage was observed at the box joints, so the TBM operator increased pressure of the main jack to prevent further leakage. Meanwhile, an intermediate jacking station (IJS) was installed as shown in **Fig. 14** in case the subsequent jacking force continued to increase. The IJS experienced the highest friction resistance at the beginning of its deployment with almost 5000 kN as shown in **Fig. 10**. After the height of the sealing rubber was readjusted, the water leakage was resolved, and the high jacking force reduced. The IJS was not used again after then. The presence of water leakage and subsequent repair measures also give rise to anomalous variations in the friction resistance gradient, as depicted in **Fig. 11**.

Beyond a jacked length of 175 m, a huge decrement in the $F_{friction}$ was observed (**Fig. 10**). The decrease in $F_{friction}$ contributed to the negative friction resistance gradient shown in **Fig. 11**. One possible explanation for this observation is that the decrement of earth pressure acting on the box crown due to the dissipation of lubricant after a long work stoppage of five days (during the new year holiday). During the jacking process, the injection and dissipation of lubricant can cause the box string lifted and sunk, resulting in the change of earth pressure acting on the top of the box. The long shutdown can cause the reduction of pressure in the overcutting gap. In this situation, the soil above the box culvert is more likely to move towards the top slab of the box and be subjected to shear resistance under the action of the shear band, resulting in positive soil arching and minimum vertical earth pressure (Terzaghi, 1936). **Fig. 15** shows the positive soil arching model. A reduction in vertical earth pressure may finally result in decrease in frictional resistance after the new year holiday. However, the traditional Terzaghi silo model does not consider lubricant injection, so it is only suitable for calculating earth pressure after a long work stoppage or during the tunnel operation when the lubricant has largely dissipated (Zhang et al., 2016). Therefore, for the jacking construction with continuous lubricant injection, it is desirable to consider the negative soil arching effect. Han et al. (2017) state that the volume and pressure of lubricant in the overcutting area will remain high during jacking process, and excess lubricant in the annulus clearance tends to leak out along the open cracks in the soil. For this project, the low permeability of mud screen generated around the box may have prevented the lubricant in the overcut from being drained into the surrounding soil by groundwater. As a result, the lubricant injection caused an increase in pressure on the outer wall of the box, which in turn pushed the supporting soil layer upward, forming a negative soil arching and maximum vertical earth pressure as shown in **Fig. 16**. To support the overburden undergone a transition from negative soil arching to positive soil arching during new year holiday, an analysis of frictional resistance will be conducted in the subsequent chapters, please refer to Section 4.3.3.

In addition, after the lubricant injection process was restarted following the holiday, it was difficult to quickly restore the lubricant volume and pressure in the annulus to its pre-holiday level. This could result in the persistence of a positive soil arching, leading to a prolonged period of low $F_{friction}$ levels. After injecting lubricant over approximately 200 m, the volume and pressure of the lubricant in the overcutting gap gradually increased. As a result, an increase in $F_{friction}$ was observed due to the re-formation of a negative soil arch. Meanwhile, the trend of skin friction (τ) can also reflect the decrease in $F_{friction}$ during new year holiday: τ steadily decreased to less than 2 kPa after a jacked distance of 175 m. It is worth to note that the $F_{friction}$ and skin friction had a certain increase near the end of the drive to over 6500 kN and 2 kPa respectively, as the TBM approached the concrete wall of reception shaft. The significant rise in the friction resistance gradient within this chainage interval, as depicted in **Fig. 11**, also corroborated this observation. One possible explanation for this occurrence is the frequent daily check stoppages that increased the average of the measured $F_{friction}$.

3.2 Deviations in alignment

Deviations in alignment are inevitable during box jacking project especially for curved route. Large deviations from line may cause the increase in the overall jacking force. As already described in (McCabe et al., 2012), some huge increases in required jacking load were observed if there were some large deviations in alignment during pipe jacking process. **Fig. 17** illustrates the trajectory deviation in this project, determined using recorded data of specific box culverts. The analysis of the horizontal deviation shows that two parts of the curved jacking route deviated from the line to a certain degree in the corresponding direction. Moreover, both horizontal and vertical deviations were found to be smaller than the recommended threshold proposed by Cheng et al. (2018). Specifically, Cheng suggested that deviations less than 60 mm would have minimal or negligible effect on jacking forces, and therefore such deviations will not be considered in this study.

3.3 Stoppages

During the TBM shutdown, such as for box culvert installation, overnights, daily check, weekends, and maintenance, there is potential for lubricant to consolidate in the overcutting gap. When jacking process restart after a stoppage, external forces are required to make the solidified lubricant flow again, which can lead to localized peaks in the frictional resistance. By analyzing the real-time curve of P_{face}, it was found that the value of F_{face} is almost not affected by work stoppages. Therefore, we only consider the effect of stoppages on $F_{friction}$. **Fig. 18** shows a zoomed-in example of $F_{friction}$ peaks for consecutive stoppages with varying shutdown time.

The increase in restart $F_{friction}$ against jacked distance for every individual stoppage is represented in **Fig. 19**. $F_{friction}$ increase was calculated as the restart $F_{friction}$ minus the $F_{friction}$ immediately before the stoppage. In order to reduce the duration, there were no Saturday stoppages during weekends. For Ougi-dori project, stoppages were categorized on the basis of duration (t) as follows: 50 min $< t <$ 1.5 h for box culvert installation; 2 h $< t <$ 5 h for lunch breaks and daily checks; 12 h $< t <$ 20 h for overnight stoppages and $t >$ 35 h for weekends. As stated above, the TBM experienced the longest shutdown of up to five days during the new year holiday, which resulted in an abnormal decrease in jacking force. Therefore, the data point related to this period was excluded from subsequent stoppage analysis. It is worth noting that the restart frictional resistance upon recommencement of jacking was usually greater than that before the last stoppage. However, some negative values were registered on **Fig. 19**, which may indicate a more conservative driving style upon resuming jacking when the stoppage was less than 1.5 hours. For long stoppages ($t >$ 12 h), the $F_{friction}$ increase required was positively correlated with jacked length, proving that it is a frictional phenomenon. While increases in $F_{friction}$ were observed for short stoppages, the increased value gradually stabilized at lower level with drive length increasing, indicating that the duration of stoppages has little effect on $F_{friction}$ required up to about 50 min-1.5 h. Furthermore, **Fig. 20** summarizes the peak values of frictional resistance caused by stoppages exceeding 1.5 hours. An overall increase of approximately 18% in $F_{friction}$, on average, was observed after the stoppages.

Fig. 21 illustrates the corresponding increases in frictional stress for each time category, revealing that the required increases in $F_{friction}$ is dependent on the duration of the stoppage. The increase in $F_{friction}$ caused by lunch break and daily check (about 2-4 h) was slightly larger than that of the box culvert installation. This phenomenon also was observed in (O'Dwyer et al., 2020), suggesting that the increase in $F_{friction}$ after a stoppage is not govern by differences in static and dynamic coefficients of friction.

4. Discussion

$F_{friction}$ is a significant factor affecting and consuming the jacking force especially in long drive (Ji et al., 2019b). During jacking process, jacking force applied on box culverts must be controlled under maximum permissible compressive strength of the box. Favorable jacking force may mitigate the risk of box culvert damage. Therefore, accurately predicting $F_{friction}$ is crucial for ensuring the safety of construction. An improved calculation model for $F_{friction}$ prediction will be discussed in this section based on the above data analysis.

4.1 Box-soil-lubricant contact model incorporating curved jacking route

During box jacking process, there may be five different contact status between the box culvert, surrounding soil and lubricant according to the lubricant distribution and geological conditions (Wen et al., 2020), showing in **Fig. 22**. The adopted box-soil lubrication system plays a vital role in the development of jacking forces. Lubrication cannot only reduce the box-soil interface friction coefficient, but also servers other two purposes: (a) stabilization of the overcut annulus, (b) flotation of the box culvert string (Milligan and Marshall, 1998). When there is insufficient lubrication, the lubricant may completely permeate into surrounding soil. As a result, the hole wall may collapse and the full box-soil contact occurs, which significantly increases the frictional resistance. Considering that the lubricant injection volume and pressure were adequate in Ougi-dori project, the possibility of full box-soil interaction occurring was excluded. Furthermore, the buoyancy of the box culvert string cannot be disregarded. O'Dwyer et al. (2020) pointed out that even if overcut is unstable, buoyancy may still occur because of the higher specific gravity of the soil-lubricant mixture. The idea scenario is when the buoyancy of the box is just in balance with gravity and box is centered within the bore, in which case the full box-lubricant contact occurs. For large cross-section box jacking like this project, the weight of the box is typically lower than buoyancy (Shou et al., 2010). Although ballast can be employed to make the box heavier and achieve the full box-lubricant contact (Praetorius and Schößer, 2017), considering construction cost and efficient, it was not used in this project. Therefore, the box may float upward and cling on the top of the bore, causing constant contact between the top slab of box and soil over the whole jacked length. In this case, the theoretical active earth pressure, rather than the hydrostatic pore water pressure, tends to be the contact pressure on the box crown (Zhang et al., 2022). For the bottom of the box, due to the adequate lubricant injection, the formed mud screen at the bottom may be effectively shielded from the hydrostatic pore water pressure, which can lead to the box-lubricant interaction.

Previous research has shown that the contact status between the side wall and the lateral soil is primarily governed by the geological condition and curved jacking path (Milligan and Norris, 1996; Sheil, 2021; Shou et al., 2010; Zhang et al., 2018). The crossing stratum was primarily composed of silt before a jacked length of 75 m in this project. The lateral soil could collapse on the side wall because of its weak self-supporting capability, combining with the limited lubricant volume accumulation before 75 m, resulting in three side box-soil contact during this chainage interval as illustrated in **Fig. 23**. Consequently, the soil pressed against the side wall and making the lateral contact pressure tend to active earth pressure. Beyond a jacked length of 75 m, TBM was jacked into sand with better self-supporting capability from silt, and the lubricating volume steadily accumulated as the jacked distance increases. One side box-soil contact status gradually formed as shown in **Fig. 23**.

The curved jacking route may also change the box-soil-lubricant contact status. The contact status between the box and surrounding soil in curved areas is more complicated than it is for linear jacking. There is a deflection angle between box joints in curved area, making the jacking force transferred to the next box has a lateral component perpendicular to the box axis. As shown in **Fig. 23**, beyond a chainage about 75 m, the curved area of the jacking route may result in two-side box-soil contact status.

This is due to the combined effect of buoyancy and the lateral component of the jacking force, which results in additional friction on the outside components.

4.2 Theoretical analysis of earth pressure considering lubricant injection

The initial state of the stresses around the tunnel when pipe jacking is often disturbed by overcutting. The Terzaghi silo model, established through active trap-door experiments as shown in **Fig. 24**, describes the new state of stress induced by soil relaxation after tunnel excavation (Terzaghi, 1936). The cover depth h was 3.91 m - 0.97 m (1.56B-0.39B) in this project, less than the minimum value $2B$ getting from active trap-door experiments to generate arching effect. Therefore, in the soil arching model, the shear band extends to the ground surface, and the soil above the box crown is subjected to shear resistance. The earth pressure on top slab of box can be determined by Terzaghi classical soil mechanics (Terzaghi, 1943) as shown in Eqs. (2) and (3):

$$B' = B + 2H\,tan(45 - \varphi/2) \tag{2}$$

$$\sigma_h = \frac{(B'\gamma - 2c)}{2Khtan\varphi}\left(1 - e^{-2Ktan\varphi\frac{h}{B'}}\right) + qe^{-2Ktan\varphi\frac{h}{B'}} \tag{3}$$

Where σ_h is soil pressure; c is soil cohesion; φ is soil friction angle; B' is silo width; B is box width; H is box heigh; q is surcharge load; γ is soil unit weight; h is burial depth of box crown; K is soil pressure ratio.

The traditional Terzaghi silo model does not reflect the disturbance of surrounding soil caused by lubricant injection, which might result in an underestimation of the earth pressure. Hence, it can only be used to calculate the earth pressure during tunnel operation. However, effects of lubricant injection should be considered when calculating earth pressure, as the injection volume and pressure can impact parameters such as silo width and soil friction angle (Zhang et al., 2016).

4.2.1 Parameter determination

For the drive of Ougi-dori project, due to the stratum disturbance caused by the extensive lubricant injection, the width of the silo above the box may be greater than that of a circular pipe jacking. In such a scenario, the shearing band will yield from the conners under the rectangular tunnel along oblique lines, and silo width B' equal to the spacing of shearing bands on both sides (Stein et al., 1989). In addition, lubricant injection also has an effect on soil friction angle. Ground loss caused by lubricant injection in rectangular box jacking typically up to dozens of millimetres, which much higher than the critical value of 10 mm suggested by J. H. Atkinson (1981). In this situation, it is expected that the majority of the soils in the shear band will reach the critical state after experiencing sufficient shearing displacement. Therefore, it is recommended to use the critical friction angle φ in this study.

There are also other parameters for earth pressure calculation need to be determined that do not affect by lubricant injection. The soil pressure ratio K equalling unity is recommended based on previously theoretical analysis, trap-door experiment results, and numerical analysis (Chevalier et al., 2012; Dewoolkar et al., 2007; Iglesia et al., 2014; Vardoulakis et al., 1981). The frictional force along the shearing band plays a crucial role in determining the earth pressure at the box crown. The associated flow rule is often used to calculate the frictional coefficient in Terzaghi arching models. However, since the associated flow rule is not able to capture the plastic characteristic of soil (Mitchell and Soga, 2005), Evans (1983) introduced the non-associated plastic flow rule to the Terzaghi arching models to better describe the relationship between the shearing stress and normal stress, as represented by Eq. (4):

$$\tau' = \sigma \frac{\cos\psi \sin\varphi}{1-\sin\psi \sin\varphi} \tag{4}$$

Where ψ is soil dilation angle, which can be defined as $\psi = \varphi - 30°$ (Ong et al., 2018; Peerun et al., 2019). For Ougi-dori project, the dilation angle decreases to zero when critical friction angle was used. Therefore, friction coefficient τ' along the shearing band is transformed from $\tan\varphi$ to $sin\varphi$.

In conclusion, the following assumptions can be considered reasonable based on the discussion above: (1) The silo width is equal to the width of the shearing band on both sides; (2) Instead of using the peak friction angle or an excessively conservative half-value, the critical friction angle should be used; (3) The soil pressure ratio should be set to 1; (4) The friction coefficient should be converted from $\tan\varphi$ to $sin\varphi$; (5) The effect of the ground load can be neglected.

4.2.2 Modified models for earth pressure based on analysis of lubricant injection

The box string is lifted and sunk during the process of the lubricant injection and dissipation, causing changes of earth pressure acting on the top of the box. An upward shearing stress will be generated at the interface of silo as the mobilized soil within the silo moves downward in relation to the stationary soil. This stress redistribution is often referred to as a positive soil arching. On the contrary, when this part of mobilized soil moves upward relative to the surrounding portions, negative soil arching will develop at the interface (Han et al., 2017).

During the new year holiday, the lubricant continued to dissipate. Although the lubricant injection was re-implemented after the resumption of construction, the injection pressure and volume in the annulus clearance were difficult to return to the previous level in a short time, resulting in the tendency of the soil overlaying the box to move toward the box roof. In this case, the positive soil arching occurs, and the vertical earth pressure reaches the lower limit as illustrated in **Fig. 15**. Substituting the re-selected parameters into Eqs. (2) and (3) and recognizing that the earth pressure is at its lower limit, the following equality can be obtained:

$$B' = B + 2H\,tan(45 - \varphi/2) \tag{5}$$

$$\sigma_{hn} = \frac{(B'\gamma_n - 2c)}{2h_n sin\varphi}\left(1 - e^{-2sin\varphi\frac{h_n}{B'}}\right) + \sigma_{hn-1}e^{-2sin\varphi\frac{h_n}{B'}} \tag{6}$$

Where σ_{hn} is the vertical earth pressure of the n^{th} stratum (kPa); h_n is the thickness of the n^{th} stratum (m). σ_{hn-1} can be regarded as the external load at the top of the next layer.

On the other hand, the injection pressure in the annulus clearance was maintained at a relatively high level during the normal jacking process. An intact mud screen was formed around the box due to sufficient injection, which prevented the lubricant in the annulus from being taken away by the groundwater in time. In addition to increasing pressure on the outer wall of the box, the injection of lubricant also caused the supporting soil layer to push upwards, resulting in negative soil arching, as illustrated in **Fig. 16** (Han et al., 2017). In this circumstance, the soil within the silo tends to slide upward, while its upward movement is restrained by the friction in the shearing band, causing the earth pressure to reach its upper limit. Thus, Eqs. (2) and (3) can be adapted as follows:

$$B' = B + 2H\,tan(45 - \varphi/2) \tag{7}$$

$$\sigma_{hn} = \frac{(B'\gamma_n - 2c)}{2h_n sin\varphi}\left(e^{2sin\varphi\frac{h_n}{B'}} - 1\right) + \sigma_{hn-1}e^{2sin\varphi\frac{h_n}{B'}} \tag{8}$$

Before a jacked distance of 75 m, the lateral soil could collapse on the box wall, which caused the sidewalls to contact the lateral soil through the lubricant and resisted the active earth pressure. The magnitude of the active earth pressure acting on the sidewalls can be calculated using the Terzaghi classical soil mechanics method as follows:

$$P_{side} = (\sigma_h + \frac{H\gamma}{2})K_a - 2c\sqrt{K_a} \tag{9}$$

Where $K_a = tan^2(45 - \varphi/2)$; Considering the influence of groundwater, the natural weight of the soil layer above the phreatic water surface and the effective weight of the soil layer below the water surface was used in the following calculation.

The lower and upper limits of vertical earth pressure with jacking distance are shown in **Fig. 25**, which were calculated by substituting the geological condition into

Eqs. (5)-(9). The variation in cover depth along the jacked length of this project leads to corresponding changes in the earth pressure acting on the box crown. The maximum and minimum of upper limits of the vertical earth pressure were calculated as 58.03 kPa and 10.58 kPa, respectively. And the corresponding limiting values of lower limit obtained by the positive soil arching model were 40.77 kPa and 10.18 kPa, separately. Earth pressure calculations will be used in frictional resistance prediction for rectangular box jacking in the next section.

4.3 Estimation of frictional resistance

As documented above, the box-lubricant-soil contact condition affects the frictional resistance around the box. Based on the contact status between the box and the surrounding soil, two main calculation models have been used to determine the frictional resistance in practice: the full contact model and the partial contact model. The surrounding soil will collapse and contact the pipes if the overcutting clearance is unstable, especially in soft soil. For this circumstance, the full soil-pipe contact model was suggested by researchers to predict jacking force (O'reilly and Rogers, 1987), which was subsequently adopted by pipe jacking standards and handbooks (ASCE, 2001; FSTT, 2006; JMTA, 2000; PJA, 1995). However, it is found that when lubricant is applied, the frictional resistance calculated by the full contact model is significantly higher than the measurement value recorded in actual engineering practice. Therefore, current research focuses on the development of partial contact model (Khazaei et al., 2004; Shimada et al., 2004; Shou et al., 2010; Zhang et al., 2018). Although many researchers have modified existing partial contact models for rectangular box jacking (JIAO et al., 2020; Ma et al., 2022; Wen et al., 2020), these models do not accurately reflect the actual contact status between the box, lubricant, and soil.

The establishment of partial contact models depends on the pipe-soil contact status, which requires the analysis of both the soil pressure on the pipe surfaces and lubricating effect (Cheng et al., 2018; Ye et al., 2020). Thus, modified calculation approaches will be developed using improved partial contact models established in Section 4.1 to predict the $F_{friction}$.

4.3.1 Composition analysis of friction force

The total frictional resistance consists of the box-soil friction resistance and box-lubricant friction resistance. The friction resistance between box string and surrounding ground is defined as Eq. (10), which can be determined by the earth pressure σ, dynamic coefficient of friction μ and contact area S_{bs} between box and soil contact interface.

$$f_{bs} = \sigma\mu S_{bs} \tag{10}$$

The earth pressure acting on the box has been determined in Section 4.2, and the contact interface area S_{bs} is equal to the box-soil contact length on cross section multiplied by the jacked distance. Without lubrication, dynamic coefficient of friction can be determined by frictional angle between soil and pipe external surface. However, when the lubrication is applied, the friction coefficient mainly depends on the properties of the lubricant (Zhang et al., 2022). The back-analysis method is commonly employed for determining the friction coefficient in pipe-jacking, supported by case studies (Cheng et al., 2018; Choo and Ong, 2020). By utilizing the box-soil contact model developed in this study, along with the drive details and calculated earth pressure, the calculated friction coefficient can be derived, as shown in **Fig. 26**. The obtained friction coefficient through back-analysis was 0.13 on average. It should be noted that the back-analysis for friction coefficient exclusively considered the measured $F_{friction}$ up to a jacked distance of 60 m. This is because the nearly linear behavior of the $F_{friction}$ within this section, and no abnormal conditions (e.g., water leakage or changes in contact status) or curved jacked routes that could impact the back-analysis were observed. Furthermore, considering the high friction resulting from the non-lubricated TBM shield dragging along the bottom of the overcut at the beginning of drive, the measurements of $F_{friction}$ for the first 10 m were excluded from back-analysis. It is essential to clarify that the premise of the back-analysis is the availability of an existing reliable box-soil contact model. The established box-soil interaction model used for back-analysis of friction coefficient was based on the analysis of jacking force, lubricant performance and TBM operating parameters. Consequently, it is necessary to conduct further verification to validate the calculated friction coefficient. The laboratory test is a reliable method for determining the friction coefficient of different lubricant (Choo and Ong, 2020; Shou et al., 2010). Ma et al. (2022) reported the use of two-component consolidated lubricant (same lubricant as this project) as a lubricating material between box culverts and soil in three box jacking projects in the Greater Tokyo Area. To evaluate its lubricating properties, laboratory tests were conducted, recommending a friction coefficient of $\mu = 0.13$, which is consistent with the results obtained from the aforementioned back-analysis. Based on the similar geological conditions and lubrication materials shared by the Ougi-dori project and the three projects reported by Ma, the calculated friction coefficient of 0.13 can be deemed appropriate for the box-soil interface.

Another component of the total friction force is the box-lubricant friction resistance. The lubricant used in this project is a kind of non-Newtonian fluid with thixotropy, which means that it will lose some of its viscosity and turn liquid under the shearing effect of the box wall during the jacking process. Hence, different from the box-soil frictional resistance which belongs to solid-solid friction, the box-lubricant friction belongs to solid-liquid friction. In this case, the bore-lubricant-box system can be simplified into a hydrodynamic parallel-plate model as shown in **Fig. 27**, and Herschel-Bulkley rheological model can be introduced to calculate box-lubricant friction.

Without considering the pressure gradient along the jacking direction, the velocity of lubricant flow $u(y)$ between two parallel plates can be expressed as Eq. (10) (Gerhart et al., 2016):

$$u(y) = \frac{V}{d} y' \tag{11}$$

Where d is the thickness of lubricant; V is the jacking speed. Additionally, it is conceivable that in the low shearing rate range, the pseudoplastic flow is superior to the plastic flow pattern in describing the lubricant flow characteristics. (Zhang et al., 2022) developed the revised Herschel-Bulkley rheological model for the calculation of the shear stress using the pseudoplastic flow pattern of the box jacking lubricant, which can be defined as follows:

$$\tau = \tau_y + k\Upsilon^n \tag{12}$$

Where τ is shear stress (Pa); k is consistency index ($Pa \cdot s^n$); n is flow index (s^{-1}). τ_y is limit dynamic shear stress, lubricant begins to flow only when shear stress exceeds the limit dynamic shear stress, which is the same as static shear stress in plastic flow patterns; $\Upsilon = du/dy'$ represents the shear rate of the lubricant. The calculation parameter of shearing stress τ_y, k and n is defined as Eq. (13), θ_{600}, θ_{300}, θ_3 represent 600 rpm, 300 rpm, and 3 rpm readings of the Fann viscometer, respectively (Zhang et al., 2022). It can be seen from Eqs. (12) and (13) that when the lubricant formulation is determined, the friction resistance between the box and the lubricant is only related to the jacking speed and lubricant thickness.

$$\begin{cases} \tau_y = 0.511\theta_3 \\ k = 0.511(\theta_{300} - \theta_3)/511^n \\ n = 3.322\, lg[\,(\theta_{600} - \theta_3)/(\theta_{300} - \theta_3)] \end{cases} \tag{13}$$

By substituting the Eq. (11) into Eq. (12), frictional resistance f_{bl} between the box and the lubricant can be obtained as follows:

$$f_{bl} = \tau S_{bl} = \left(\tau_y + k\left(\frac{V}{d}\right)^n\right) S_{bl} \tag{14}$$

Where S_{bl} is the contact area between the box and the lubricant, which is equal to box-lubricant contact length on cross section multiplied by jacked distance.

4.3.2 Friction resistance calculation models for curved box jacking

The Ougi-dori project consisted of three straight-line segments and two curved line segments. The three linear sections shown in **Fig. 2** are categorized according to drive length (m) as follows: linear jacking section 1 (LS1) was from the launch shaft to measurement point BC1 (58.405 m); linear jacking section 2 (LS2) was from the measurement point EC1 to BC2 (41.546 m); linear jacking section 3 (LS3) was from measurement point EC2 to the reception shaft (11.057 m). Similarly, the two curved sections can be categorized as follows: curved jacking section 1 (CS1) was from measurement point BC1 to EC1 (45.093 m); curved jacking section (CS2) was from measurement point BC2 to EC2 (64.872 m). The friction resistance of linear jacking sections can be directly calculated by the combination of Eqs. (10) and (12) as

$$F_f^{LS} = f_{bs} + f_{bl} = \sigma\mu S_{bs} + \left(\tau_y + k\left(\frac{V}{d}\right)^n\right) S_{bl} \tag{15}$$

Before a jacked distance of 75 m, sidewalls and the top slab in linear section 1 were assumed in contact with the ground through lubricant, causing three-side box soil interaction. Furthermore, the overcutting area in LS2 and LS3 was presumed to be able to maintain its stability, and one-side box-soil interaction occurs. Therefore, for linear jacking section, S_{bs} changes with the jacked length L as

$$\begin{cases} S_{bs} = (B + 2H) \cdot L & L \le 75m \\ S_{bs} = B \cdot L & L > 75m \end{cases} \tag{16}$$

Considering the earth pressure acting on the top and side walls was different, the friction resistance around the rectangular box for LS1 can be calculated by Eq. (17):

$$F_f{}^{LS1} = f_{bs}^{LS1} + f_{bl}^{LS1} = \sigma\mu B L_{S1} + 2P_{side}\mu H L_{S1} + \left(\tau_y + k\left(\frac{V}{d}\right)^n\right) B L_{S1} \tag{17}$$

Similarly, Eqs. (18) and (19) can be employed to calculate the frictional resistance of LS2 and LS3.

$$F_f{}^{LS2} = f_{bs}^{LS2} + f_{bl}^{LS2} = \sigma\mu B L_{S2} + \left(\tau_y + k\left(\frac{V}{d}\right)^n\right)(2H + B)L_{S2} \tag{18}$$

$$F_f{}^{LS3} = f_{bs}^{LS3} + f_{bl}^{LS3} = \sigma\mu B L_{S3} + \left(\tau_y + k\left(\frac{V}{d}\right)^n\right)(2H + B)L_{S3} \tag{19}$$

The determination of frictional resistance of two curved jacking segments is more complicated. Due to the friction effect of outside components in curved section of jacking path, the frictional resistance in curved area is generally higher than in linear area, which has been theoretically studied by many scholars (Broere et al., 2007; Nanno, 1996; Wei et al., 2005). JMTA (2000) proposed an empirical formula by using Terzaghi arching theory (Terzaghi, 1943) to estimate the jacking force for a general curved pipe jacking. However, numerous pipe jacking construction cases (Shou et al., 2010; Zhang et al., 2018) show that the growth ratio of frictional resistance is lower with successful lubricating system application than the fundamental JMTA prediction equation. With consideration of the lubricating effect, Khazaei et al. (2004) and Shimada et al. (2004) derived improved formulas for calculating the jacking force in curved areas using different methods: recursion and integration, respectively. Whereas their methods were deduced based on circular pipe jacking and may not be directly applicable to rectangular box jacking. Therefore, these two methods are modified as follows to make them appropriate for Ougi-dori project.

The modified Shimada method: The box culverts jacked into the ground can be assumed to be connected in a consecutive curved shape as presented in **Fig. 28**, since the radius of the curvature is extremely larger than the length of a single box. The box string in curved area keep equilibrium under the jacking force F_{total}, face resistance F_{face}, and frictional resistance $F_{friction}$.

As seen in **Fig. 29**, it was assumed that the left side of the box is affected by the soil reaction force f. With the consideration of the soil reaction, the force acting on the unit box area can be defined as illustrated in **Fig. 30**.

The force acting on the tangent direction of the box unit satisfies the equilibrium equation by substituting the Eqs. (10) and (14) as

$$(F + dF)\cos\frac{d\theta}{2} - F\cos\frac{d\theta}{2} = \mu f H R d\theta + \mu\sigma l_{bs} R d\theta + \left[\tau_y + k\left(\frac{V}{d}\right)^n\right] l_{bl} R d\theta \quad (20)$$

Where f is the soil reaction against the jacked box (kPa); l_{bs} is the box-soil contact length on box section; l_{bl} is the box-lubricant contact length on box section; θ is the angle of the curved section; R is the jacking path radius of the curvature.

Making dF the subject of Eq. (20) and recognizing that $\cos(d\theta/2)$ goes to 1 as $d\theta$ approaching to zero, the following equation is obtained

$$dF = \mu fHRd\theta + \mu\sigma l_{bs}Rd\theta + \left[\tau_y + k\left(\frac{V}{d}\right)^n\right] l_{bl}Rd\theta \tag{21}$$

The equilibrium of the force in the normal direction of the box unit is expressed by

$$(F + dF)\, sin\frac{d\theta}{2} + F\, sin\frac{d\theta}{2} = fRHd\theta \tag{22}$$

It is also conceivable that $\sin(d\theta/2)$ approaches to $d\theta/2$ if $d\theta$ goes to zero, the Eq. (22) should be applied as

$$Fd\theta + F\frac{d\theta}{2} = fHRd\theta \tag{23}$$

Assuming the term $\mathrm{dF}(d\theta/2)$ is relatively small and can be neglected, by combining Eqs. (21) and (23) gets the following form:

$$\frac{dF}{F+\sigma l_{bs}R+\frac{1}{\mu}\left[\tau_y+k\left(\frac{V}{d}\right)^n\right]l_{bl}R} = \mu d\theta \tag{24}$$

Integrating the Eq. (24) from F_{face} to F_{total} which corresponded to the angle of curved area $\theta = 0$ to $\theta = \theta$, the Eq. (24) then becomes

$$\frac{F_{total}+\sigma l_{bs}R+\frac{1}{\mu}\left[\tau_y+k\left(\frac{V}{d}\right)^n\right]l_{bl}R}{F_{face}+\sigma l_{bs}R+\frac{1}{\mu}\left[\tau_y+k\left(\frac{V}{d}\right)^n\right]l_{bl}R} = e^{\mu\theta} \tag{25}$$

Therefore, the increase ratio of the thrust λ in the curved area forward the linear jacking defined as

$$\lambda = \frac{e^{\mu\theta}-1}{\mu\theta} \tag{26}$$

From Eqs. (25) and (26), the fundamental estimation equation in the curved area can be expressed as

$$F_{total} = F_{face}e^{\mu\theta} + \lambda\left[\mu\sigma l_{bs} + \left(\tau_y + k(\frac{V}{d})\right)^n l_{bl}\right] CL \tag{27}$$

Where $CL = R\theta$ is the length of curved area.

The modified Khazaei recursive method: Force analysis on a single box culvert in the curved area can be seen in **Fig. 31**. For the first box jacked into curved section, assuming that the initial jacking force of the curved area is F_0, then the equilibrium equation of the tangenitial direction of the box is express as:

$$F_1 = F_0 \cos\Phi + \mu f' H l + \mu\sigma l_{bs} l + \left[\tau_y + k\left(\frac{V}{d}\right)^n\right] l_{bl} l \tag{28}$$

The equilibrium of the force acting on this box in the normal direction is defined as

$$f' = F_0 \sin\Phi \tag{29}$$

Considering that the angle between the box culverts in the curved area is small, the value of $\cos\Phi$ tends to 1. Combination of Eqs. (28) and (29) yields the jacking force of first box in curved area express as

$$F_1 = F_0 + \mu H l F_0 \sin\Phi + \mu\sigma l_{bs} l + \left[\tau_y + k\left(\frac{V}{d}\right)^n\right] l_{bl} l \tag{30}$$

Similarly, it can be proved that the jacking force of the second box in curved area is given by

$$F_2 = F_0(1 + \mu \sin\Phi)^2 + 2\left[\mu\sigma l_{bs} l + \left[\tau_y + k\left(\frac{V}{d}\right)^n\right] l_{bl} l\right] \tag{31}$$

By analogy, we can obtain the jacking force of the m^{th} box in curved area as

$$F_{total} = F_0(1 + \mu \sin\Phi)^m + m\left[\mu\sigma l_{bs} l + \left(\tau_y + k\left(\frac{V}{d}\right)^n\right) l_{bl} l\right] \tag{32}$$

In this study, only frictional resistance will be discussed subsequence, and according to the jacking force composition, the friction force can be obtained as $\sum F_{friction} = F_{total} - F_{face}$.

4.3.3 A comparison of measured and theoretical values of frictional resistance

After establishing the estimation formulas, the theoretical friction resistance was calculated. The partial calculation parameters in Ougi-dori project are shown in **Table 4**. To verify the accuracy of the established contact model, we applied the PBK formula to calculate the $F_{friction}$ and compared calculations with measured data. The PBK formula, developed by Pellet-Beaucour and Kastner (2002), can be used to estimate the jacking force using the Terzaghi silo model, which was then invoked by (Choo and Ong, 2015, 2020; Ong et al., 2018) for this purpose. **Fig. 32** compares the calculations of the PBK formula and the measurement data plotted against the jacked distance: note that the computation incorporates the peak earth pressure and average penetration rate for each jacking section. Furthermore, the PBK formula for calculating $F_{friction}$ is specifically designed for circular pipe jacking and is therefore not suitable for this project. Instead, the PBK earth pressure calculation method (Pellet-Beaucour and Kastner, 2002) was utilized to determine the earth pressure. The computed PBK earth pressure values were subsequently used in Eq. (33) to estimate the $F_{friction}$, which is shown in **Fig. 32**. The use of the three-side box-soil contact status in calculations yields results that are more consistent with the measurements for jacked distance before 75 m, due to the greater friction force caused by this contact status. After comparing the measured and calculated values for distances before 75 m and 75-175 m, it was observed that the rate of increase in $F_{friction}$ decreased by 1.5 times for the measured data, while the calculated rate of increase in $F_{friction}$ using the PBK method decreased by 1.2 times. It is noteworthy that the calculation of the measured data was adjusted to exclude abnormal increases in frictional resistance beyond 75 m, which could have resulted from water leakage at the box joint. Despite the potential impact of water leakage on the development of frictional resistance, the rate of increase in measured $F_{friction}$ was found to be comparable to the rate of increase in calculated $F_{friction}$. Therefore, it can be considered that the one-side box-soil contact status gradually formed beyond 75 m, due to the accumulation of lubricant in the overcutting clearance, leading to a more pronounced lubrication effect. Thus, beyond 75 m of jacking, selecting the one-side box-soil interaction for calculations is more appropriate, as it better reflects the reduction in actual frictional resistance. Regarding the jacked length beyond 175 m, due to the impact of the new year holiday, it will be analysed later in this section.

Although the PBK formula has demonstrated effectiveness in predicting friction resistance, supporting the validity of the contact model developed in this study. However, the work of Pellet-Beaucour and Kastner (2002) did not consider the effect of the lubricant injection-dispersion process on frictional resistance. As a result, the PBK formula may not accurately predict the changes in frictional resistance due to the lubricant injection and dissipation. Therefore, it is more appropriate to incorporate the positive and negative soil arching model into the calculation of frictional resistance.

As shown in **Fig. 33**, we compared the calculated $F_{friction}$ values of the Shimada method and Khazaei method for the upper limit of earth pressure. The calculation results, which was based on three-side box-soil contact model for a jacked distance of less than 75 m, shows that the calculated $F_{friction}$ using upper limit of earth pressure provides a better fit with the measurements than the PBK method. Furthermore, the comparison of the Shimada method and the Khazaei method reveals that the predicted values from each method exhibit similar accuracy. The calculated value obtained using the Khazaei method is slightly higher than that of the Shimada method, and this difference becomes increasingly apparent as the length of the curved section increases as illustrated in **Fig. 33**(b). One possible explanation for this result is that the Shimada method simplifies the box train as a circular arc, which leads to a reduction in the surface area of box-soil contact used in calculation and consequently, a slightly lower calculated value.

The Khazaei method is limited to box jacking projects with a single curvature radius and may not be applicable to projects with varying curvature trajectories, as it is difficult to obtain the specific angle change for each box. To ensure the calculations in this paper are more general and applicable to a wider range of projects, the focus will be exclusively on the Shimada method. To evaluate the impact of the curve section on the friction force, this study evaluates the contribution of additional friction force in the CS2 section to the overall frictional resistance, as depicted in **Fig. 34**. The results indicate that the additional friction generated in the curved section has little effect on the calculated value of the total friction. Therefore, it can be concluded that the curve segments with a curvature radius of more than 100 m can be approximated as linear jacking, with the additional friction ignored. After the TBM entered CS2 for a certain period, it was observed that the measured value was slightly higher than the calculated value. One possible reason for this phenomenon is that the TBM encountered obstacles, such as large pebbles or woodpiles. **Fig. 9** illustrates that near 160 m, the construction time per box increased from an average of 1 hour to 1.5 hours, and the TBM operator increased the current of the cutterhead and reduced the penetration velocity, as shown in **Fig. 8**. These changes in operating parameters can be attributed to possible obstacles encountered at 160 m, which prompted the operator to take corresponding measures.

The comparison between the measured and calculated $F_{friction}$ using Shimada method after 75 m is presented in **Fig. 35**. The measured value of the frictional resistance fluctuates within the upper and lower limits of calculated value. After the new year holiday (beyond 175 m), both the measured and calculated $F_{friction}$ decreased by 34% and 31%, respectively. This indicates that the model established in this study is effective in reflecting the change in $F_{friction}$ resulting from the transition of the overburden from negative arching (due to injected lubricant) to positive arching (due to drained lubricant). Moreover, this transition can be considered to occur across the entire drive, as the drop rate of $F_{friction}$ is calculated from the cumulative jacked distance and frictional resistance, which reflects changes along the entire drive.

As the TBM neared the reception shaft, an increase in the measured data was observed. This increase may have been caused by the re-injection of lubrication after the jacking process was restarted, which resulted in an increase in pressure in the overcutting gap and the reappearance of negative soil arching. Furthermore, at the jacked distance beyond 215 m, the measured value exceeded the calculated value, possibly due to the frequent daily check stoppages that increased the average of the measurements as the TBM approached the concrete wall of the reception shaft as shown in **Fig. 9**. This phenomenon has been observed in various projects reported by other scholars (O'Dwyer et al., 2020; Zhang et al., 2022).

5. Concluding remarks and implications for practical engineering

This paper presents an interpretation of data obtained from a Japan box-jacking project conducted in silt and silty sand. A modified box-soil-lubricant interaction model is then established based on the analysis of the tunnelling parameters. The proposed contact model is applied to forecast jacking force using the modified Shimada and Khazaei methods. The main conclusions drawn from this study are as follows:

(a) Detailed monitoring of construction sites is of paramount importance, as it can reveal significant differences in driving style and tunnelling characteristics as the TBM pass through different soil. As the TBM encounters harder soil, operators often adjust the cutterhead torque and penetration velocity, potentially influencing the development of face pressure.

(b) Frictional resistance between box and soil is often the main contribution to the total jacking force during long drives, which is closely linked to their mutual interaction. Varied geological conditions can give rise to dissimilar states of contact between box and soil. During the initial phase of the Ougi-dori project, due to the soft soil condition and the limited accumulation of lubricant in the annular clearance, the lateral soil is contact with the side wall, resulting in the three-sided box-soil interaction and a relatively high rate of increase in frictional resistance before a jacked distance of 75 m.

(c) As the construction progresses, the lubricant volume and pressure gradually increase in the overcutting area, leading to the formation of a complete mud screen and stabilizing the hole wall. The box string remains suspended in jacking process, and the one-sided box-soil interaction becomes the dominant contact state, which reduces the rate of increase in frictional resistance after 75 m.

(d) The impact of stoppages on frictional resistance is highly time-dependent, particularly beyond approximately 1.5 hours. The observed elevation in skin friction after stoppages manifests a positive correlation with the jacked distance, implying that it may be a frictional phenomenon. However, the increment in frictional resistance augments with the duration of stoppages, indicating that the phenomenon cannot be attributed to a difference between kinetic and static friction coefficients. Conducting a detailed study on lubricant performance is essential to elucidate the underlying mechanisms behind such frictional resistance increases.

(e) During the process of lubricant injection and dissipation, the box string is assumed to be elevated and sunk in the hole, thereby giving rise to positive and negative soil arching that affect the vertical earth pressure. The jacking process was interrupted for a period of five days during the new year holiday. Throughout this hiatus period, the lubricant in the overcutting area continued to dissipate, leading to the gradual control of vertical earth pressure by positive soil arching. Consequently, the friction resistance remained at a lower level. Following the resumption of the injection process, the frictional resistance gradually reverts to its former higher level, comparable to the level before the shutdown.

(f) A formula for calculating the total frictional resistance of curved box-jacking was established by modifying Shimada and Khazaei's method. In comparison to the PBK method currently employed in the industry, the proposed formula yielded significantly improved predictions of monitored data. Furthermore, the study ascertained that in curved box-jacking with a curvature radius surpassing 100 meters, the additional resistance generated by the curve section has a negligible impact on the total jacking force.

This study underscores the efficacy of retroactive analysis of drive data, a valuable but underutilized resource within the current box-jacking industry. It should also be noted that the results outlined in this paper pertain to specific TBM and soil/lubrication conditions. Meanwhile, the friction prediction method proposed in this study may have limitations in predicting variations in friction under exceptional circumstances, such as water leakage at pipe joint, resumption following a long stoppage, or frequent stoppages during the drive of a single box. Thus, further refinement and validation of the proposed calculation model are necessary to enable its application to more complex scenarios.

6. List of notations

N:	Uncorrected standard penetration test value
N_a:	Average value of uncorrected standard penetration test
F_{total}:	Total jacking force
F_{face}:	Force acting on the face of the TBM
$F_{friction}$:	Frictional resistance between structure and the surrounding soil
P_{face}:	Average earth pressure acting on the face of the TBM
P_{side}:	Active earth pressure acting on the box sidewalls
B:	Box width
H:	Box height
B':	Silo with
q:	Surcharge load of ground surface
h:	Cover depth
h_n:	The thickness of the n^{th} stratum
γ:	Soil unit weight
γ_n:	Soil unit weight of the n^{th} stratum
σ:	Earth pressure
σ_h:	Vertical earth pressure
σ_{hn}:	Vertical earth pressure of the n^{th} stratum
c:	Soil cohesion
φ:	Critical friction angle
K:	Soil pressure ratio
ψ:	Soil dilation angle
τ:	Shear stress
τ':	Friction coefficient along the shearing band
K_a:	Active earth pressure coefficient
μ:	Dynamic coefficient of friction

u: Velocity of the lubricant flow

d: Thickness of lubricant

k: Consistency index of the lubricant

n: Flow index of the lubricant

Υ: The shear rate of the lubricant

τ_y: Limit dynamic shear stress

θ_{600}: 600 rpm reading of the Fann viscometer

θ_{300}: 300 rpm reading of the Fann viscometer

θ_3: 3 rpm reading of the Fann viscometer

f: Soil reaction against the jacked box

f': Force acting on single box in the normal direction

f_{bl}: Frictional resistance between box and lubricant

f_{bs}: Frictional resistance between box and soil

L: Jacked length

l: Length of single box culvert

l_{bs}: Box-soil contact length on box culvert cross section

l_{bl}: Box-lubricant contact length on box culvert cross section

S_{bs}: Contact area between box and soil contact interface

S_{bl}: Contact area between box and lubricant contact interface

θ: Angle of the curved jacking section

R: Jacking path radius of the curvature

Φ: Angle between box culverts for curved area

m: m^{th} box in curved area

CL: Length of curved area

λ: Increase ratio of the jacking force in curved area forward linear jacking

F_0: Initial jacking force of the curved jacking area

F_f^{LS}: Frictional resistance of linear jacking sections

F_f^{LS1}: Total frictional resistance of linear jacking section 1

F_{bs}^{LS1}: Box-soil frictional resistance of linear jacking section 1

F_{bl}^{LS1}: Box-lubricant frictional resistance of linear jacking section 1

F_f^{LS2}: Total frictional resistance of linear jacking section 2

F_{bs}^{LS2}: Box-soil frictional resistance of linear jacking section 2

F_{bl}^{LS2}: Box-lubricant frictional resistance of linear jacking section 2

F_f^{LS3}: Total frictional resistance of linear jacking section 3

F_{bs}^{LS3}: Box-soil frictional resistance of linear jacking section 3

F_{bl}^{LS3}: Box-lubricant frictional resistance of linear jacking section 3

References

ASCE, 2001. Standard Practice for Direct Design of Precast Concrete Pipe for Jacking in Trenchless Construction. American Society of Civil Engineering, Reston, Virginia. https://doi.org/10.1061/9780784413081

Beckmann, D., Stein, R., Fabri, T., Uhlenbroch, A., 2007. CoJack - A new statics method of computing and controlling pipe jacking. Tunn. Undergr. Space Technol. 22, 587-599. https://doi.org/10.1016/j.tust.2007.02.006

Bergeson, W., 2014. Review of long drive microtunneling technology for use on large scale projects. Tunn. Undergr. Space Technol. 39, 66-72. https://doi.org/10.1016/j.tust.2013.02.001

Broere, W., Faassen, T.F., Arends, G., van Tol, A.F., 2007. Modelling the boring of curves in (very) soft soils during microtunnelling. Tunn. Undergr. Space Technol. 22, 600-609. https://doi.org/10.1016/j.tust.2007.06.002

Chapman, D.N., Ichioka, Y., 1999. Prediction of jacking forces for microtunnelling operations. Tunn. Undergr. Space Technol. 14, 31-41. https://doi.org/10.1016/S0886-7798(99)00019-X

Chen, X.L., Ma, B.S., Najafi, M., Zhang, P., 2021. Long rectangular box jacking project: A case study. Undergr. Space. 6, 101-125. http://doi.org/10.1016/j.undsp.2019.08.003

Cheng, W.-C., Ni, J.C., Shen, J.S.-L., Huang, H.-W., 2017. Investigation into factors affecting jacking force: a case study. Proceedings of the Institution of Civil Engineers - Geotechnical Engineering. 170, 322-334. 10.1680/jgeen.16.00117

Cheng, W.C., Ni, J.C., Arulrajah, A., Huang, H.W., 2018. A simple approach for characterising tunnel bore conditions based upon pipe jacking data. Tunn. Undergr. Space Technol. 71, 494-504. https://doi.org/10.1016/j.tust.2017.10.002

Chevalier, B., Combe, G., Villard, P., 2012. Experimental and discrete element modeling studies of the trapdoor problem: influence of the macro-mechanical frictional parameters. Acta Geotech. 7, 15-39. https://doi.org/10.1007/s11440-011-0152-5

Choo, C.S., Ong, D.E.L., 2015. Evaluation of Pipe-Jacking Forces Based on Direct Shear Testing of Reconstituted Tunneling Rock Spoils. J. Geotech. Geoenviron. Eng. 141. http://doi.org/10.1061/(Asce)Gt.1943-5606.0001348

Choo, C.S., Ong, D.E.L., 2020. Assessment of non-linear rock strength parameters for the estimation of pipe-jacking forces. Part 2. Numerical modeling. Eng. Geol. 265. https://doi.org/10.1016/j.enggeo.2019.105405

Curran, B.G.M., Bryan A., 2011. Analysis of jacking force data for microtunnels in glacial till at Kilcock, Ireland. In: Proceedings of the 15th European Conference on Soil Mechanics and Geotechnical Engineering, Athens, 1627-1632. http://dx.doi.org/10.3233/978-1-60750-801-4-1627

Dewoolkar, M.M., Santichaianant, K., Ko, H.Y., 2007. Centrifuge modeling of granular soil response over active circular trapdoors. Soils and Foundations. 47, 931-945. https://doi.org/10.3208/sandf.47.931

Evans, C.H., 1983. An examination of arching in granular soils. Master's thesis, Massachusetts Institute of Technology, Cambridge, Massachusetts.152-204

FSTT, 2006. Microtunneling and Horizontal Drilling: Recommendations. French Society for Trenchless Technology, Newport Beach.

Gerhart, P.M., Gerhart, A.L., Hochstein, J.I., 2016. Munson, Young and Okiishi's Fundamentals of Fluid Mechanics. John Wiley & Sons, New York.

Han, J., Wang, F., Al-Naddaf, M., Xu, C., 2017. Progressive development of two-dimensional soil arching with displacement. Int. J. Geomech. 17, 04017112. https://doi.org/10.1061/(ASCE)GM.1943-5622.0001025

Iglesia, G.R., Einstein, H.H., Whitman, R.V., 2014. Investigation of Soil Arching with Centrifuge Tests. J. Geotech. Geoenviron. Eng. 140. https://doi.org/10.1061/(ASCE)GT.1943-5606.0000998

J. H. Atkinson, P.L.B., 1981. The Mechanics of Soils: An Introduction to Critical State Soil Mechanics. McGraw-Hill Book Company, New York.

Ji, X., Zhao, W., Ni, P., Barla, M., Han, J., Jia, P., Chen, Y., Zhang, C., 2019a. A method to estimate the jacking force for pipe jacking in sandy soils. Tunn. Undergr. Space Technol. 90, 119-130. https://doi.org/10.1016/j.tust.2019.04.002

Ji, X.B., Ni, P.P., Barla, M., 2019b. Analysis of jacking forces during pipe jacking in granular materials using particle methods. Undergr. Space. 4, 277-288. https://doi.org/10.1016/j.undsp.2019.03.002

JIAO, C.-l., ZHAO, X., NIU, F.-j., 2020. Pipe-Soil Contact State and Jacking Force Prediction of Rectangular Pipe Jacking. J. Northeast. Univ. 41, 1459. http://doi.org/10.12068/j.issn.1005-3026.2020.10.015

JMTA, 2000. Pipe-jacking Application. Japan Micro Tunnelling Association, Tokyo.

JSTT, 2018. Box jacking Method Design Needle in Japan. Japan Society for Trenchless Technology, Tokyo.

Kaushal, V., Najafi, M., Serajiantehrani, R., 2020. Environmental Impacts of Conventional Open-Cut Pipeline Installation and Trenchless Technology Methods: State-of-the-Art Review. J. Pipeline Syst. Eng. Pract. 11. http://doi.org/10.1061/(Asce)Ps.1949-1204.0000459

Khazaei, S., Shimada, H., Matsui, K., 2004. Analysis and prediction of thrust in using slurry pipe jacking method. In: Proceedings of the 30th ITA-AITES World Tunnel Congress, Singapore, 356. https://doi.org/10.1016/j.tust.2004.01.048

Lehmann, G., Kaesling, H., Cambier, A., Praetorius, S., Thuro, K., 2022. Performance analysis of utility tunneling data: A case study of pipe jacking in hard rock in Brittany, France. Tunn. Undergr. Space Technol. 127. https://doi.org/10.1016/j.tust.2022.104574

Li, J.B., 2017. Key Technologies and Applications of the Design and Manufacturing of Non-Circular TBMs. Engineering. 3, 905-914. https://doi.org/10.1016/j.eng.2017.12.002

Lu, H., Matthews, J., Iseley, T., 2020. How does trenchless technology make pipeline construction greener? A comprehensive carbon footprint and energy consumption analysis. J. Clean. Prod. 261, 121215. https://doi.org/10.1016/j.jclepro.2020.121215

Luo, Y., Alaghbandrad, A., Genger, T.K., Hammad, A., 2020. History and recent development of multi-purpose utility tunnels. Tunn. Undergr. Space Technol. 103. http://doi.org/10.1016/j.tust.2020.103511

Ma, P., Shimada, H., Sasaoka, T., Hamanaka, A., Moses, D.N., Dintwe, T.K.M., Matsumoto, F., Ma, B.S., Huang, S., 2022. A new method for predicting the friction resistance in rectangular pipe-jacking. Tunn. Undergr. Space Technol. 123. https://doi.org/10.1016/j.tust.2021.104338

Maehara, K., Sasaoka, T., Hamanaka, A., Shimada, H., 2019. Effect of fatty acids addition into backfilling material in over-cutting area on improvement of lubrication performance for pipe jacking. Open J. Civ. Eng. 13, 281-287. https://doi.org/10.2174/1874149501913010281

Matsumoto, K., 1998. How to use N value and c・φ, first ed ed. Soil Engineering Society, Tokyo (In Japanese).
McCabe, B., Reilly, C.C., Orr, T.L., 2012. Analysis of microtunnel jacking forces in alluvium and glacial till in Mullingar, Ireland. In: Proceedings of the World Tunnelling Conference, Bangkok.
Meskele, T., Stuedlein, A.W., 2015. Static Soil Resistance to Pipe Ramming in Granular Soils. J. Geotech. Geoenviron. Eng. 141. http://doi.org/10.1061/(Asce)Gt.1943-5606.0001237
Milligan, G.W.E., Marshall, M.A., 1998. The functions and effects of lubrication in pipe jacking, in: Ferreira, N. (Ed.), Tunnels and Metropolises 2, Balkema, Rotterdam, pp. 739-744.
Milligan, G.W.E., Norris, P., 1996. Site-based research in pipe jacking - Objectives, procedures and a case history. Tunn. Undergr. Space Technol. 11, 3-24. https://doi.org/10.1016/0886-7798(95)00041-0
Mitchell, J.K., Soga, K., 2005. Fundamentals of soil behavior. John Wiley & Sons New York.
Namli, M., Guler, E., 2017. Effect of Bentonite Slurry Pressure on Interface Friction of Pipe Jacking. J. Pipeline Syst. Eng. Pract. 8. https://doi.org/10.1061/(Asce)Ps.1949-1204.0000255
Nanno, T., 1996. A method for driving curved pipe-jacked tunnels. Tunn. Undergr. Space Technol. 11, 3-25. https://doi.org/10.1016/S0886-7798(97)00021-7
O'Dwyer, K.G., McCabe, B.A., Sheil, B.B., 2020. Interpretation of pipe-jacking and lubrication records for drives in silty soil. Undergr. Space. 5, 199-209. https://doi.org/10.1016/j.undsp.2019.04.001
O'reilly, M.P., Rogers, C.D.F., 1987. Pipe jacking forces. In: Proceedings of International Conference on Foundations and Tunnels, Edinburgh, 201.
Ong, D.E.L., Sim, Y.S., Leung, C.F., 2018. Performance of Field and Numerical Back-Analysis of Floating Stone Columns in Soft Clay Considering the Influence of Dilatancy. Int. J. Geomech. 18. https://doi.org/10.1061/(Asce)Gm.1943-5622.0001261
Peerun, M.I., Ong, D.E.L., Choo, C.S., 2019. Interpretation of Geomaterial Behavior during Shearing Aided by PIV Technology. J. Mater. Civ. Eng. 31. https://doi.org/10.1061/(Asce)Mt.1943-5533.0002834
Pellet-Beaucour, A.L., Kastner, R., 2002. Experimental and analytical study of friction forces during microtunneling operations. Tunn. Undergr. Space Technol. 17, 83-97. https://doi.org/10.1016/S0886-7798(01)00044-X
PJA, 1995. Guide to best practice for the installation of pipe jacks and microtunnels. Pipe Jacking Association, London.
Praetorius, S., Schößer, B., 2017. Bentonite handbook: Lubrication for pipe jacking. John Wiley & Sons, New York.
Reilly, C.C., Orr, T.L., 2012. Analysis of interface friction effects on microtunnel jacking forces in coarse-grained soils. In: Proceedings of the Bridge and Concrete Research in Ireland Conference, Dublin, 121-126.
Reilly, C.C., Orr, T.L.L., 2017. Physical modelling, of the effect of lubricants in pipe jacking. Tunn. Undergr. Space Technol. 63, 44-53. https://doi.org/10.1016/j.tust.2016.11.005
Sheil, B., 2021. Prediction of microtunnelling jacking forces using a probabilistic observational approach. Tunn. Undergr. Space Technol. 109. https://doi.org/10.1016/j.tust.2020.103749
Shimada, H., Khazaei, S., Matsui, K., 2004. Small diameter tunnel excavation method using slurry pipe-jacking. Geotech Geol Eng. 22, 161-186. https://doi.org/10.1023/B:GEGE.0000018365.84174.ea
Shou, K., Yen, J., Liu, M., 2010. On the frictional property of lubricants and its impact on jacking force

and soil-pipe interaction of pipe-jacking. Tunn. Undergr. Space Technol. 25, 469-477. https://doi.org/10.1016/j.tust.2010.02.009

Stein, D., Möllers, K., Bielecki, R., 1989. Microtunnelling, first ed ed. Wiley, New York.

Sterling, R.L., 2020. Developments and research directions in pipe jacking and microtunneling. Undergr. Space. 5, 1-19. https://doi.org/10.1016/j.undsp.2018.09.001

Stroud, M., 1989. The standard penetration test–its application and interpretation. In: Proceedings of Conference on Penetration Testing in the UK, London.

Sun, Y., Wu, F., Sun, W.J., Li, H.M., Shao, G.J., 2019. Two Underground Pedestrian Passages Using Pipe Jacking: Case Study. J. Geotech. Geoenviron. Eng. 145. https://doi.org/10.1061/(Asce)Gt.1943-5606.0002006

T. Hashimoto, J.B., 2004. Simultaneous backfill grouting, pressure development in construction phase and in the long-term. Tunn. Undergr. Space Technol. 19, 447. https://doi.org/10.1016/j.tust.2004.02.057

Tavakoli, R., Najafi, M., Tabesh, A., Ashoori, T., 2017. Comparison of Carbon Footprint of Trenchless and Open-Cut Methods for Underground Freight Transportation. In Pipelines 2017 : Construction and Rehabilitation, Reston, VA, 45-55. https://doi.org/10.1061/9780784480892.005

Terzaghi, K., 1936. Stress Distribution in Dry and in Saturated Sand Above a Yielding Trap-Door. In: Proceedings of the 1st International Conference on Soil Mechanics and Foundation Engineering, Cambridge, Massachusetts.

Terzaghi, K., 1943. Theoretical soil mechanics. John Wiley & Sons New York.

Valdenebro, J.V., Gimena, F.N., 2018. Urban utility tunnels as a long-term solution for the sustainable revitalization of historic centres: The case study of Pamplona-Spain. Tunn. Undergr. Space Technol. 81, 228-236. https://doi.org/10.1016/j.tust.2018.07.024

Vardoulakis, I., Graf, B., Gudehus, G., 1981. Trap-Door Problem with Dry Sand - a Statical Approach Based Upon Model Test Kinematics. Int. J. Numer. Anal. Methods Geomech. 5, 57-78. https://doi.org/10.1002/nag.1610050106

Wei, G., Xu, R.Q., Yu, J.Y., Wang, Z., 2005. Site-based experimental study on pipe behavior during pipe jacking. Rock Soil Mech. 26, 1273-1277. http://doi.org/10.11779/CJGE201710012

Wen, K., Shimada, H., Zeng, W., Sasaoka, T., Qian, D.Y., 2020. Frictional analysis of pipe-slurry-soil interaction and jacking force prediction of rectangular pipe jacking. Eur. J. Environ. Civ. Eng. 24, 814-832. http://doi.org/10.1080/19648189.2018.1425156

Ye, Y.C., Peng, L.M., Zhou, Y., Yang, W.C., Shi, C.H., Lin, Y.X., 2020. Prediction of Friction Resistance for Slurry Pipe Jacking. Appl. Sci. 10. http://doi.org/10.3390/app10010207

Zhang, H.F., Zhang, P., Zhou, W., Dong, S., Ma, B.S., 2016. A new model to predict soil pressure acting on deep burial jacked pipes. Tunn. Undergr. Space Technol. 60, 183-196. https://doi.org/10.1016/j.tust.2016.09.005

Zhang, P., Behbahani, S.S., Ma, B.S., Iseley, T., Tan, L.X., 2018. A jacking force study of curved steel pipe roof in Gongbei tunnel: Calculation review and monitoring data analysis. Tunn. Undergr. Space Technol. 72, 305-322. https://doi.org/10.1016/j.tust.2017.12.016

Zhang, Y.L., Feng, X., Zhou, H., Zhang, P., Ma, B.S., Tan, L.X., Wang, J.F., 2022. Pressure characteristics of rectangular box jacking considering box-soil-lubricant interaction. Tunn. Undergr. Space Technol. 126. https://doi.org/10.1016/j.tust.2022.104569

List of Tables:

Table 1 Technical specifications of the deployed EPB pipe-jacking machine.

EPB pipe-jacking machine	
Cutting head type	Soil
Lining type	Box jacking
Cutting diameter (mm)	3370 * 2570
Inner diameter (mm)	2800 * 1800
Load main bearing (kN)	3400
Revolution nominal torque (kNm)	1091.5
Max. revolution (rpm)	1.28
Rotation nominal torque (kNm)	272.9
Max. rotation (rpm)	5.12
Min. turning radius (m)	60
Weight (t)	65

Table 2 Soil properties.

Soil	Thickness (m)	N_a	Unit weight ($kN \cdot m^{-3}$)	Critical friction angle (φ)	Cohesion (kPa)
Made ground	1.9-2.5	3	16	15	15
Sand	2.5-4.8	25	20	35	0
Peat	5.3	2	14	10	15
Silt	3.1-5	1	14	10	15
Silt sand	1.1-3.9	6	17	25	0
Sandy silt	1-4.1	7	16	15	30

Table 3 Standard formulation for the two-component consolidated lubricant

Two-component consolidated lubricant	
A-component:	B-component:
36 L (2 cans total 50 kg)	1 bag total 20 kg
Add 164 L of water	Add 191 L of water
Total 200 L	Total 200 L

Table 4 Calculation parameters of frictional resistance.

Parameters	Jacking section				
	LS1	CS1	LS2	CS2	LS3
σ_{upper} (kPa)	53.03	52.95	50.03	40.03	15.41
σ_{lower} (kPa)	39.77	39.73	38.24	32.83	12.07
σ_{PBK} (kPa)	46.44	46.40	44.63	38.18	13.53
V (mm/min)	47.37	44.05	39.04	36.14	26.52
θ (°)		25.84		37.17	
CL (m)		45.09		64.87	
λ		1.03		1.03	
Φ (°)		0.73		0.73	
m		35		51	
μ			0.13		
d (mm)			35		
θ_{600}			178		
θ_{300}			120		
θ_{3}			8		

List of Figures:

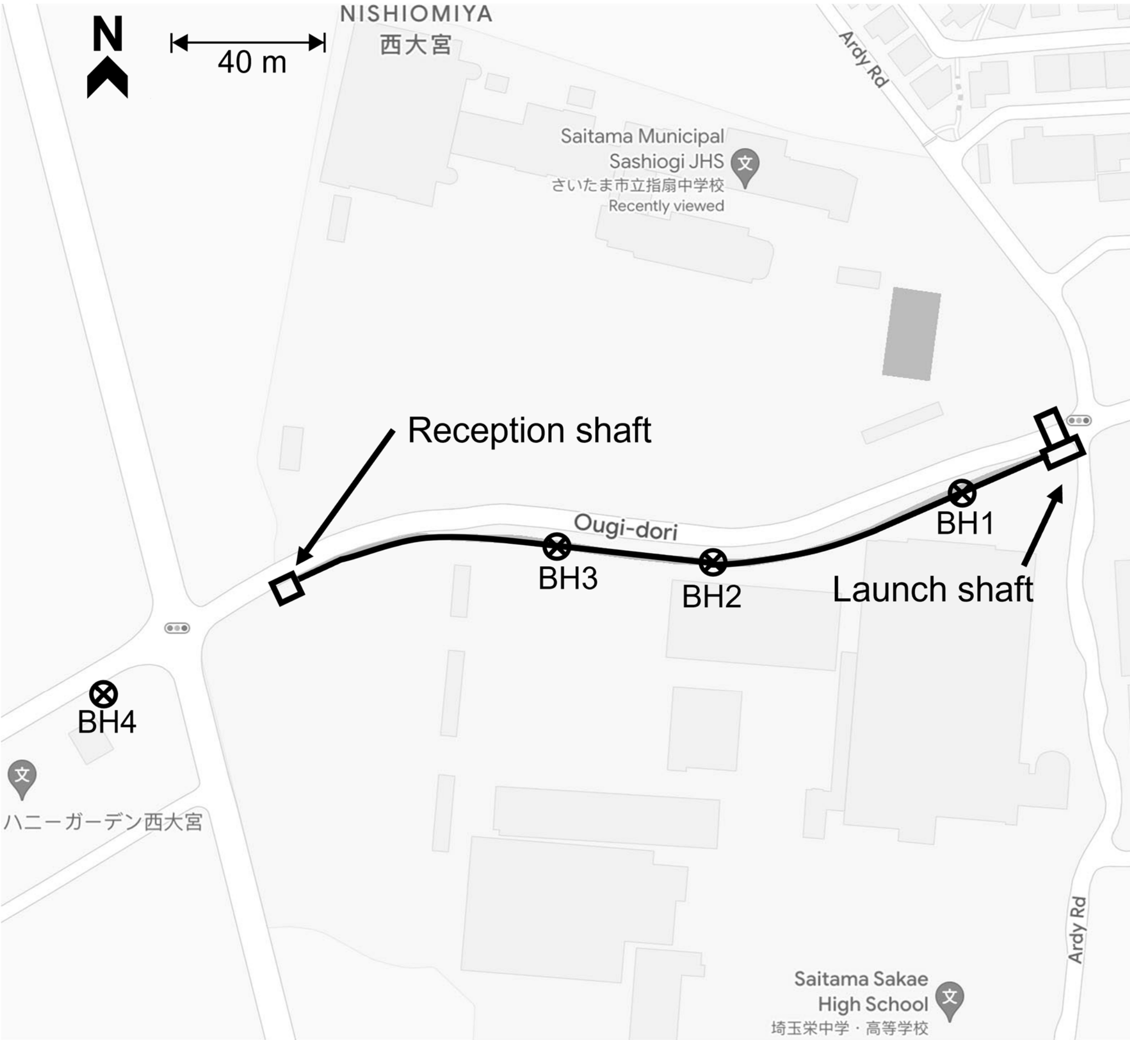

Fig. 1 Location of tunnel and shafts at Ougi-dori site (adapted from Google Maps).

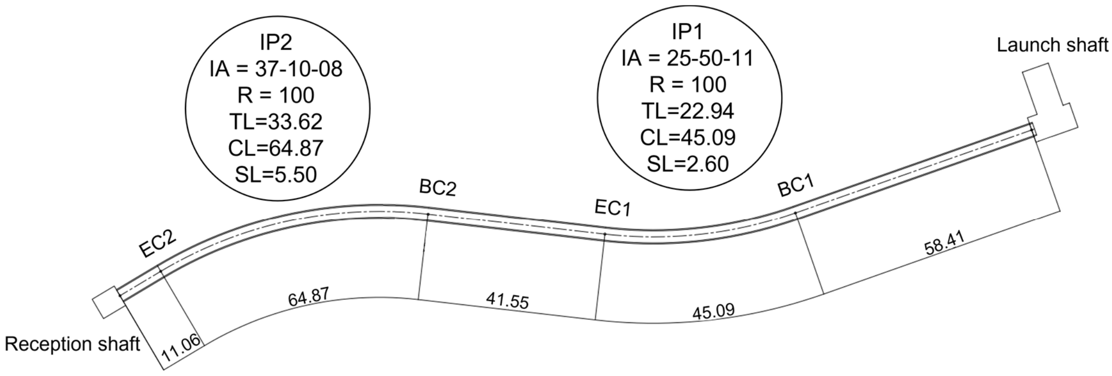

Fig. 2 Route condition of Ougi-dori project.

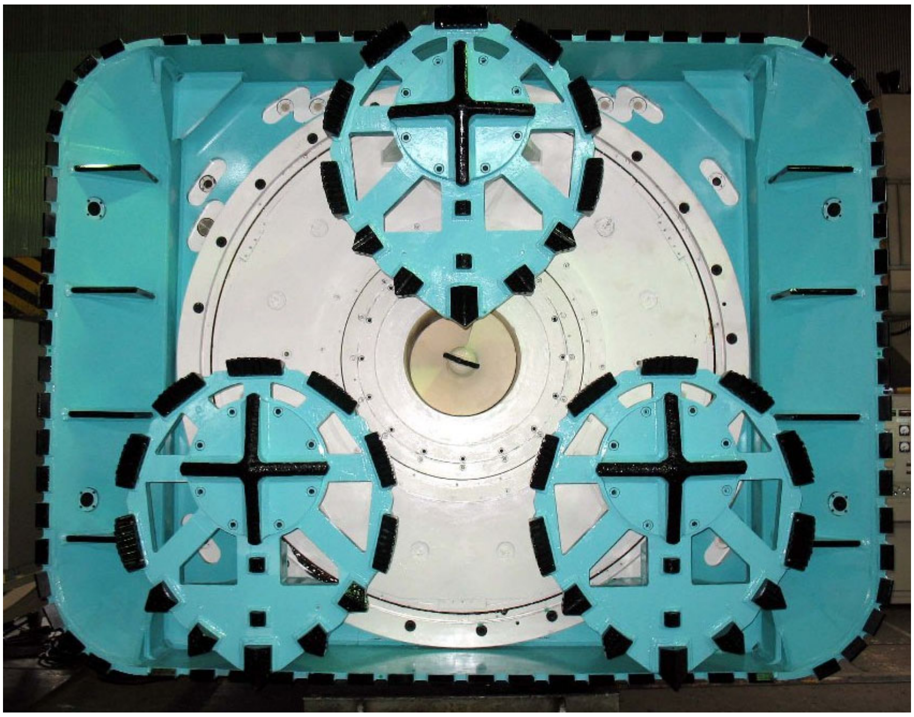

(a) Excavating system with three rotational cutterhead

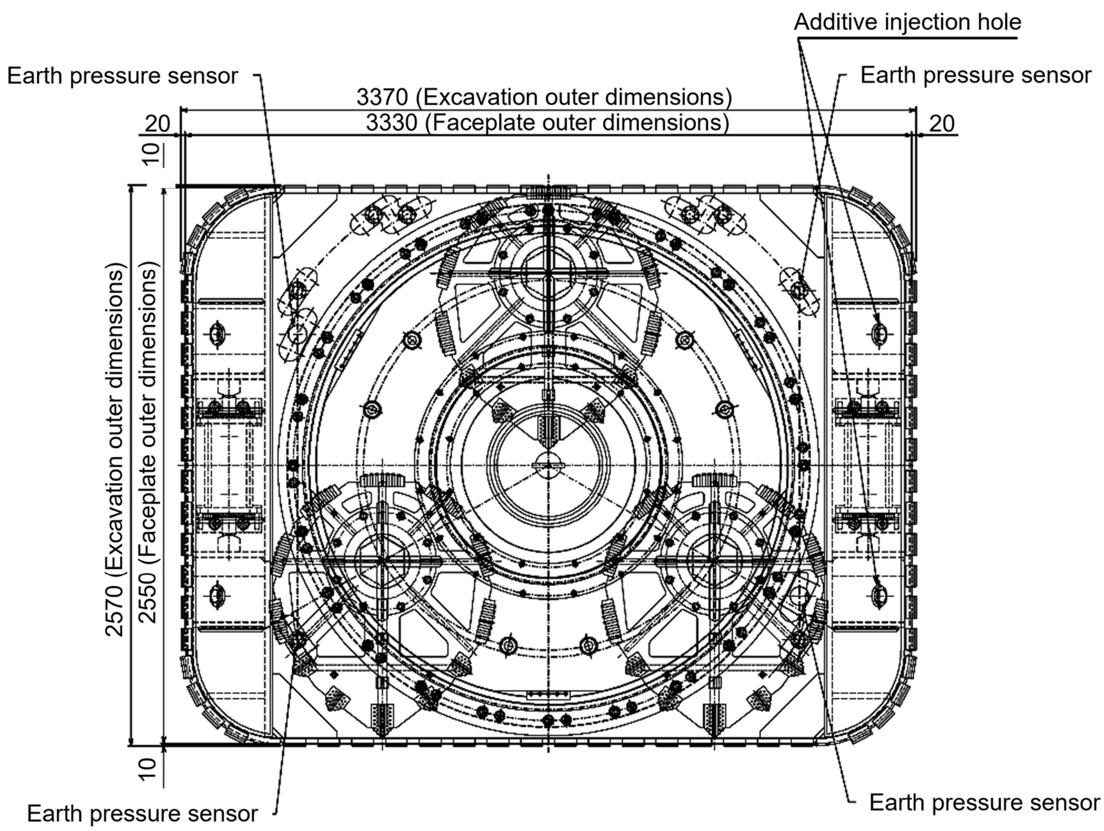

(b) Design diagram

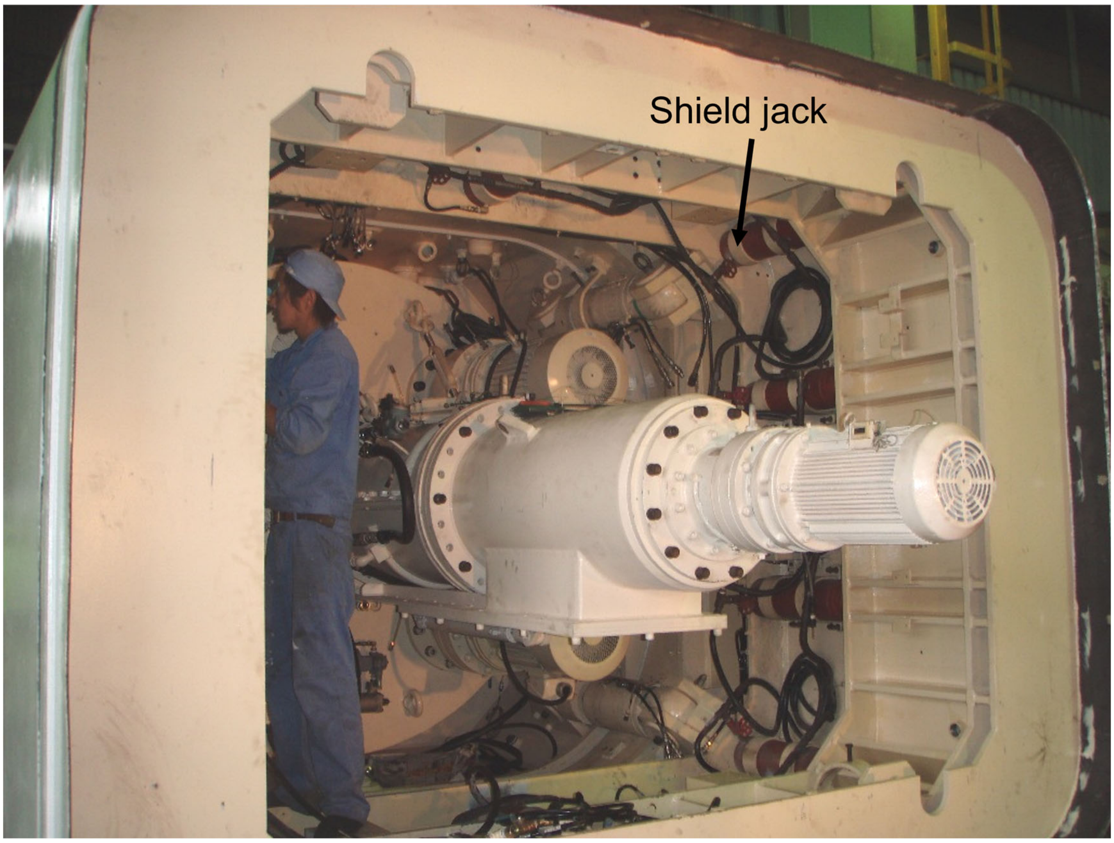

(c) Shield jack system

Fig. 3 Diagrams of the box jacking machine.

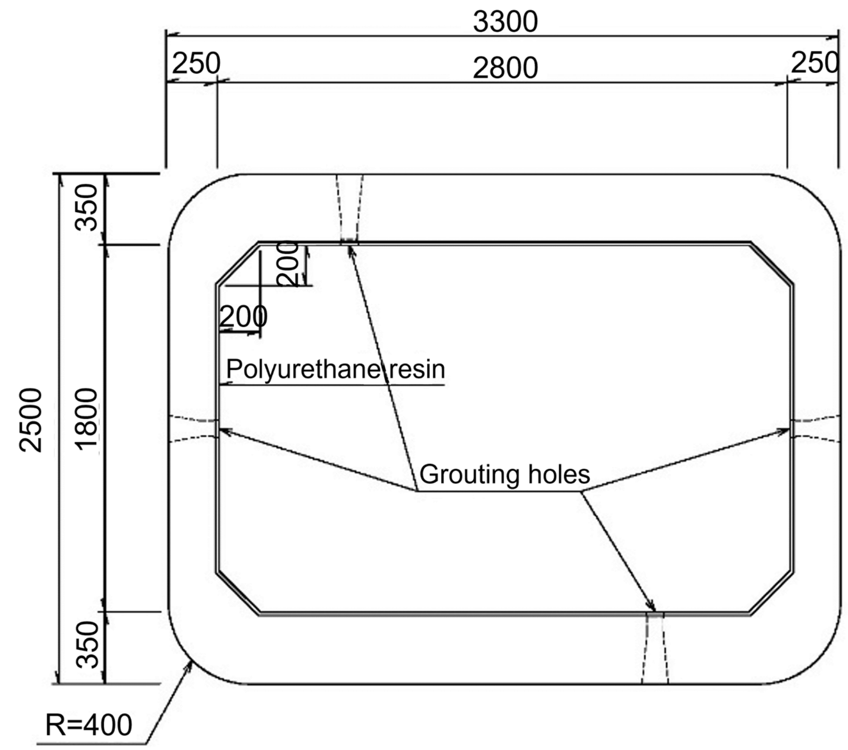

(a)Diagrammatic corss-section

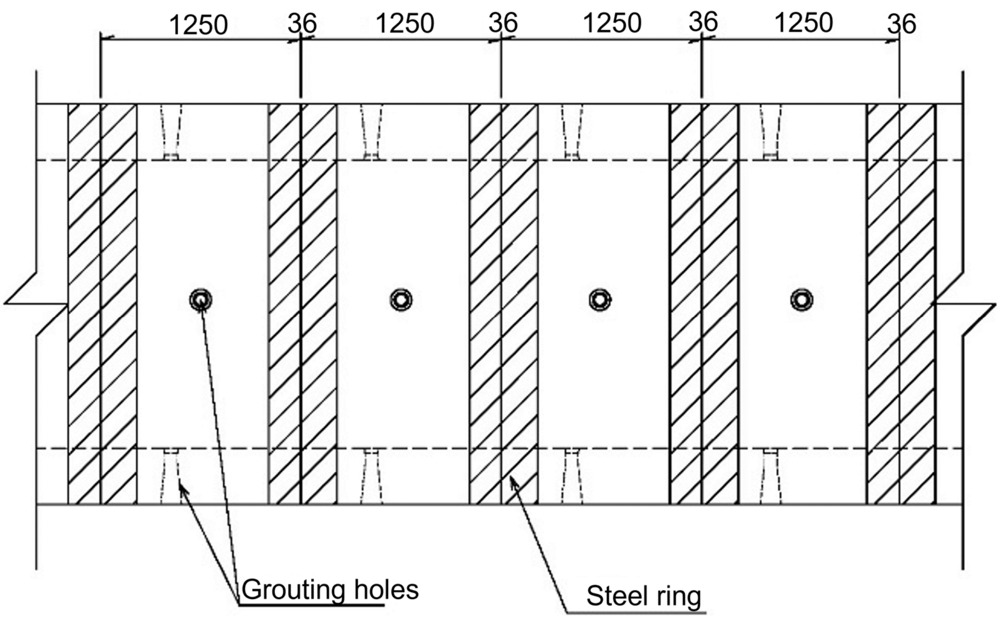

(b) Diagrammatic side elevation

(c) Box culvert

Fig. 4 Schematic diagram of the box culvert.

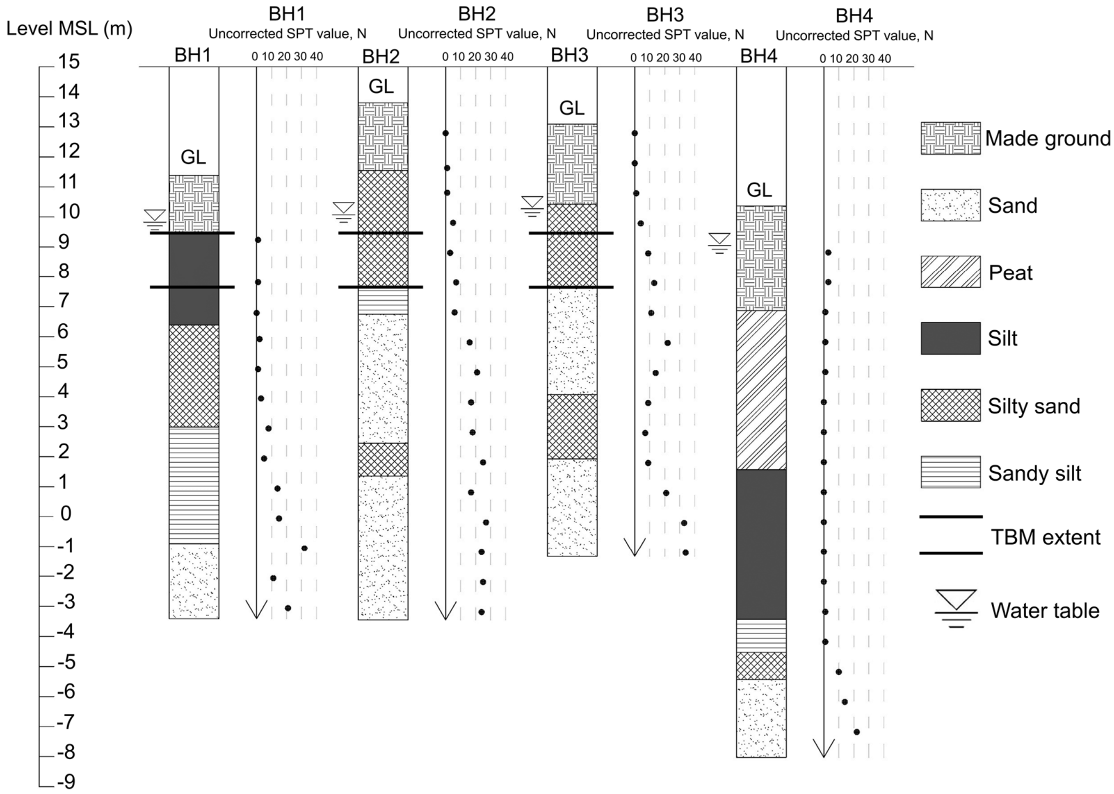

Fig. 5 Stratigraphy and uncorrected SPT profiles.

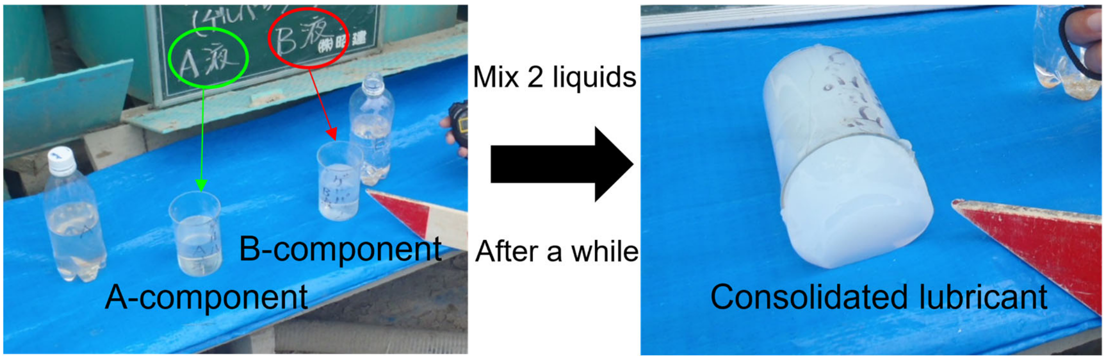

Fig. 6 Consolidation Process of the two-component consolidated lubricant.

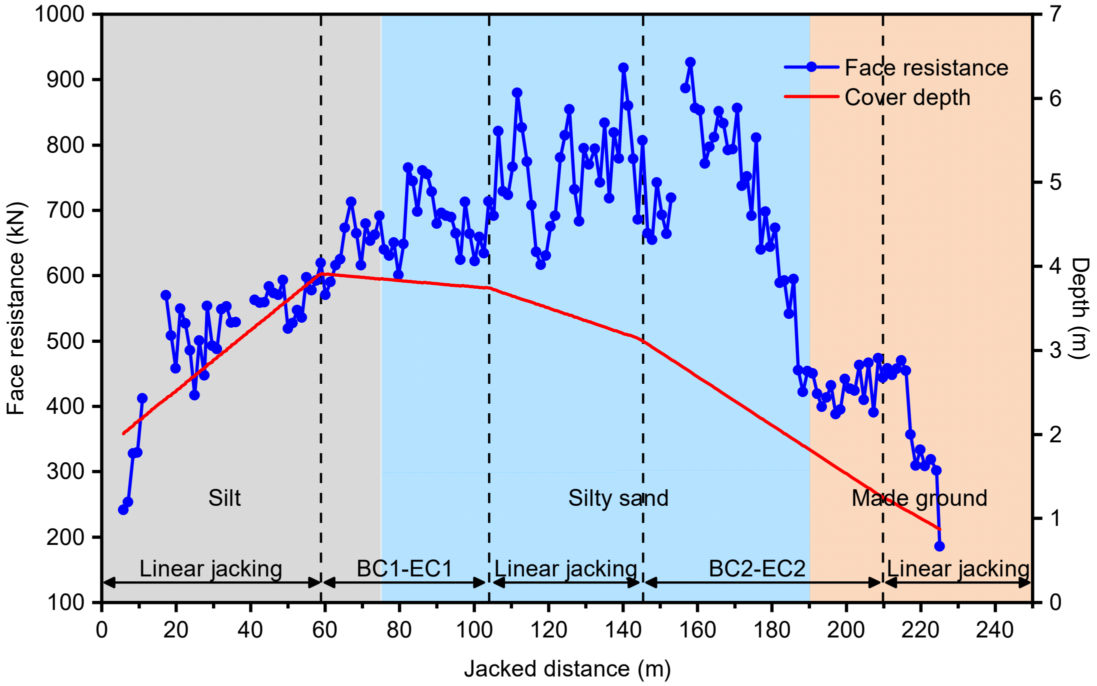

Fig. 7 Face resistance and cover depth against jacked distance.

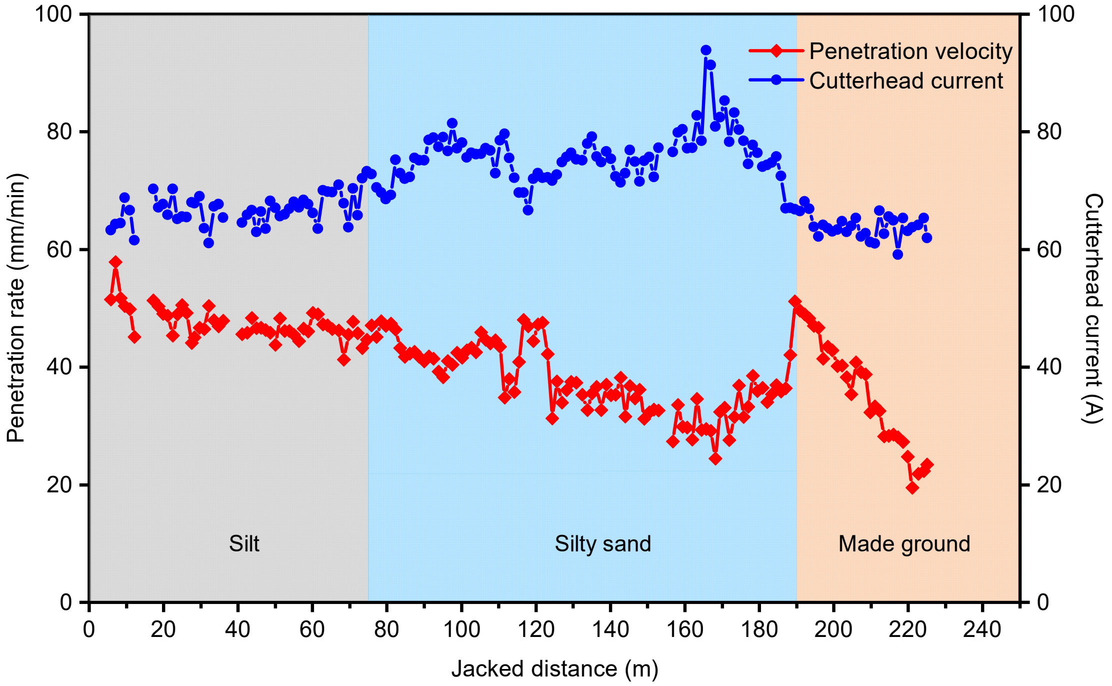

Fig. 8 Developments of cutterhead current and penetration rate.

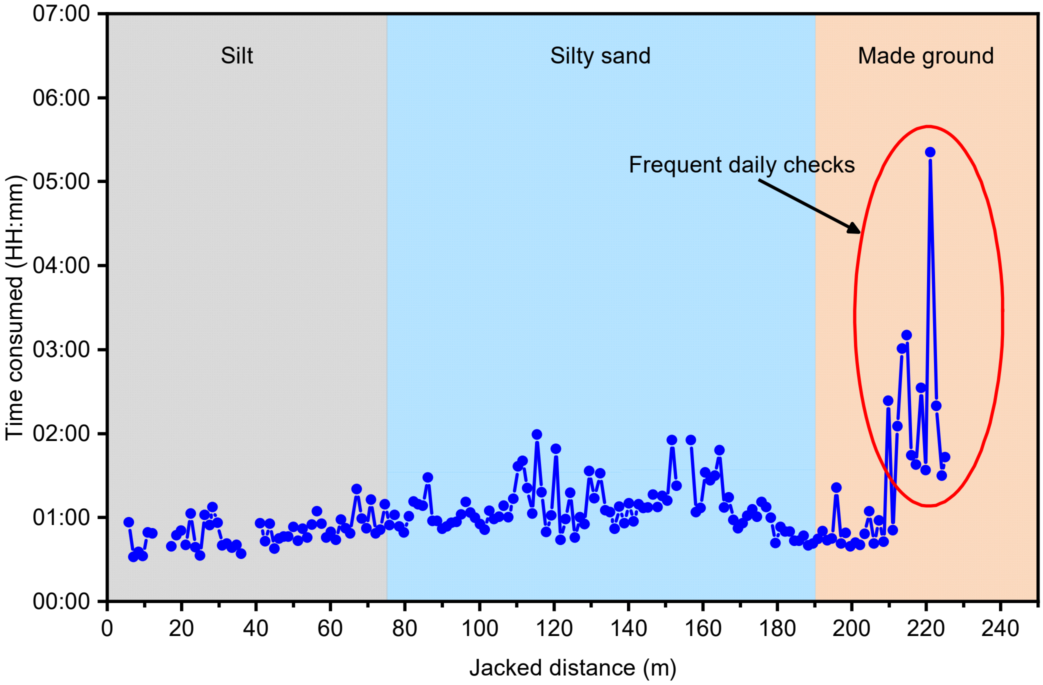

Fig. 9 Time consumed by jacking each box culvert.

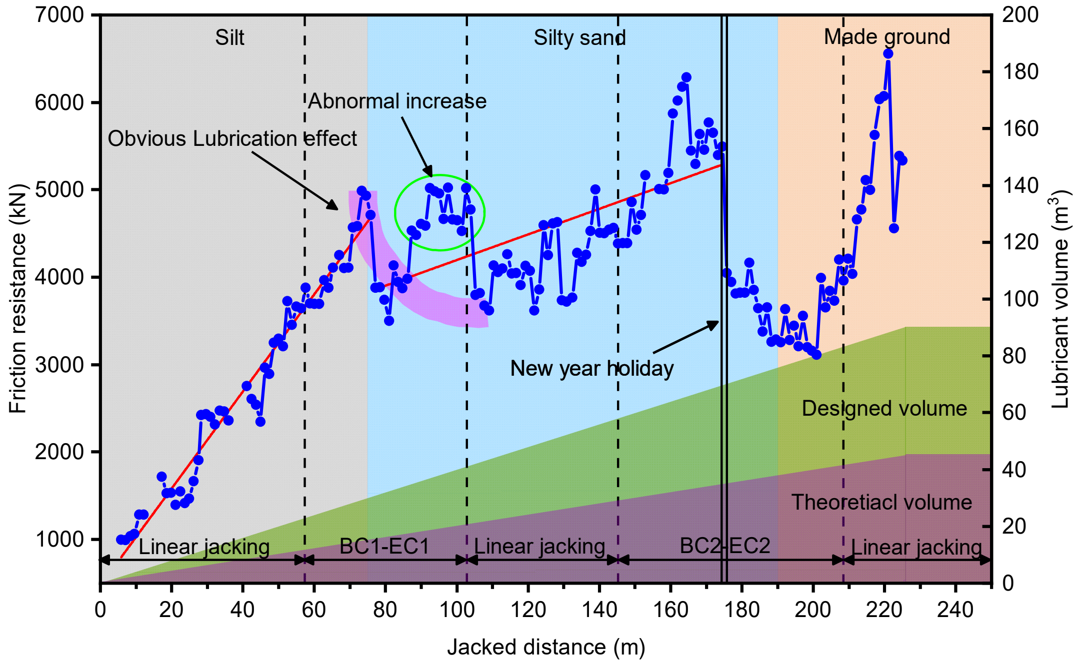

Fig. 10 Development of frictional resistance.

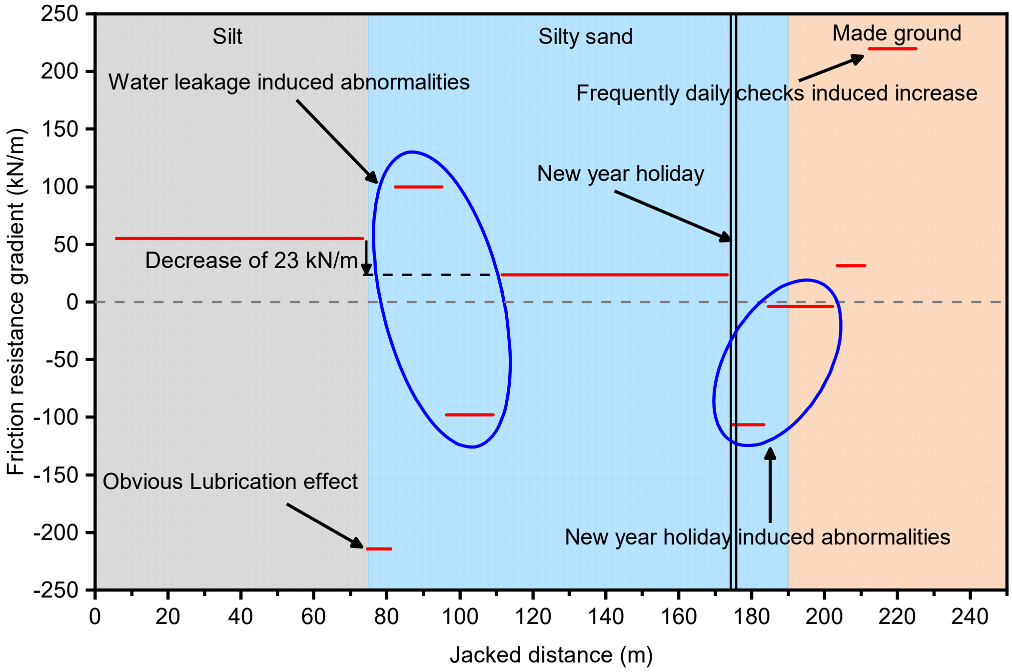

Fig. 11 Relationship between jacked distance and friction resistance gradient.

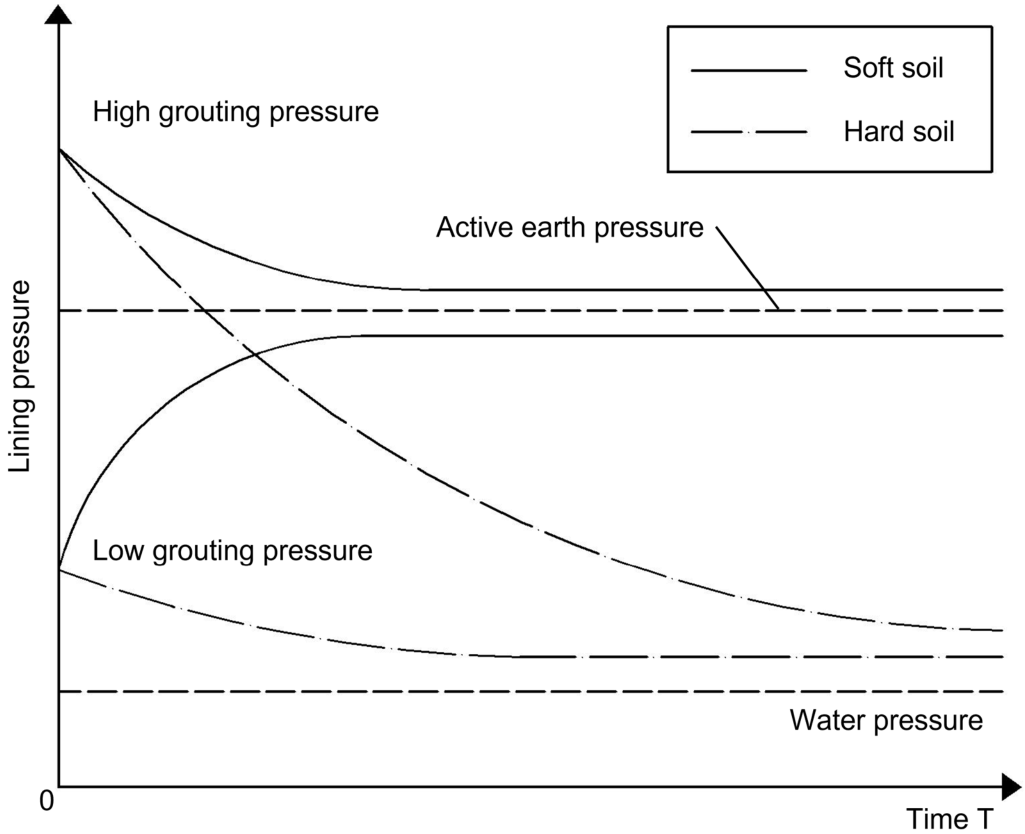

Fig. 12 The variation curve of contact pressure in different stratum (Hashimoto and Brinkman (2004).

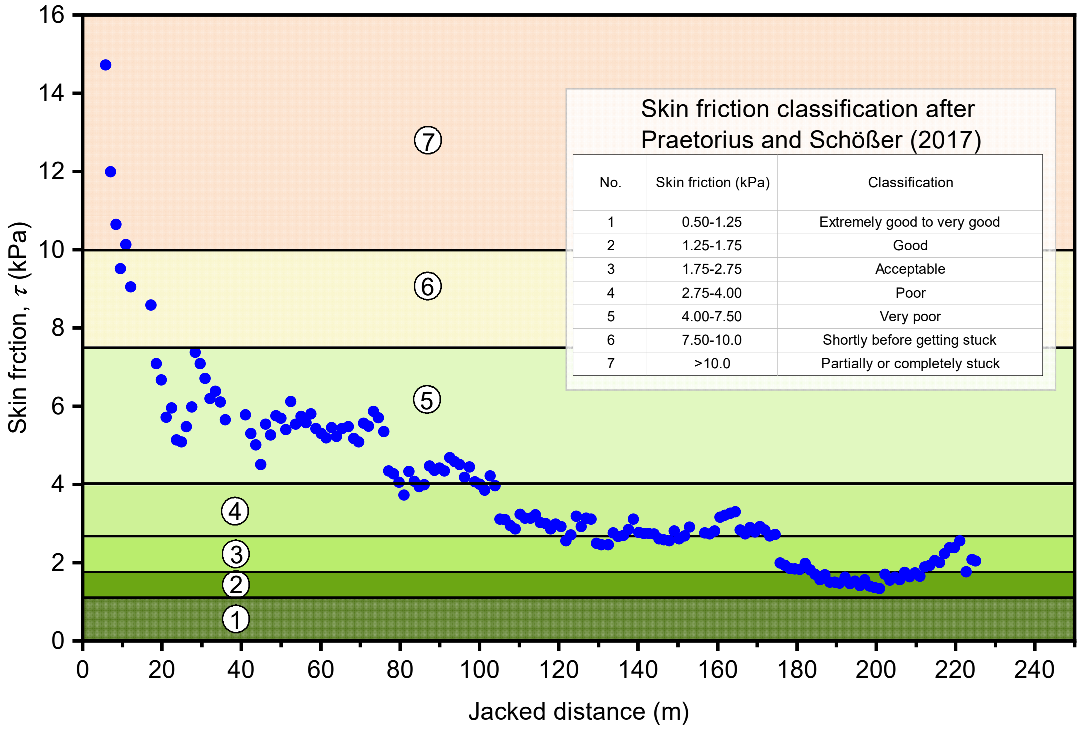

Fig. 13 Skin friction.

Fig. 14 Rectangular intermediate jacking station.

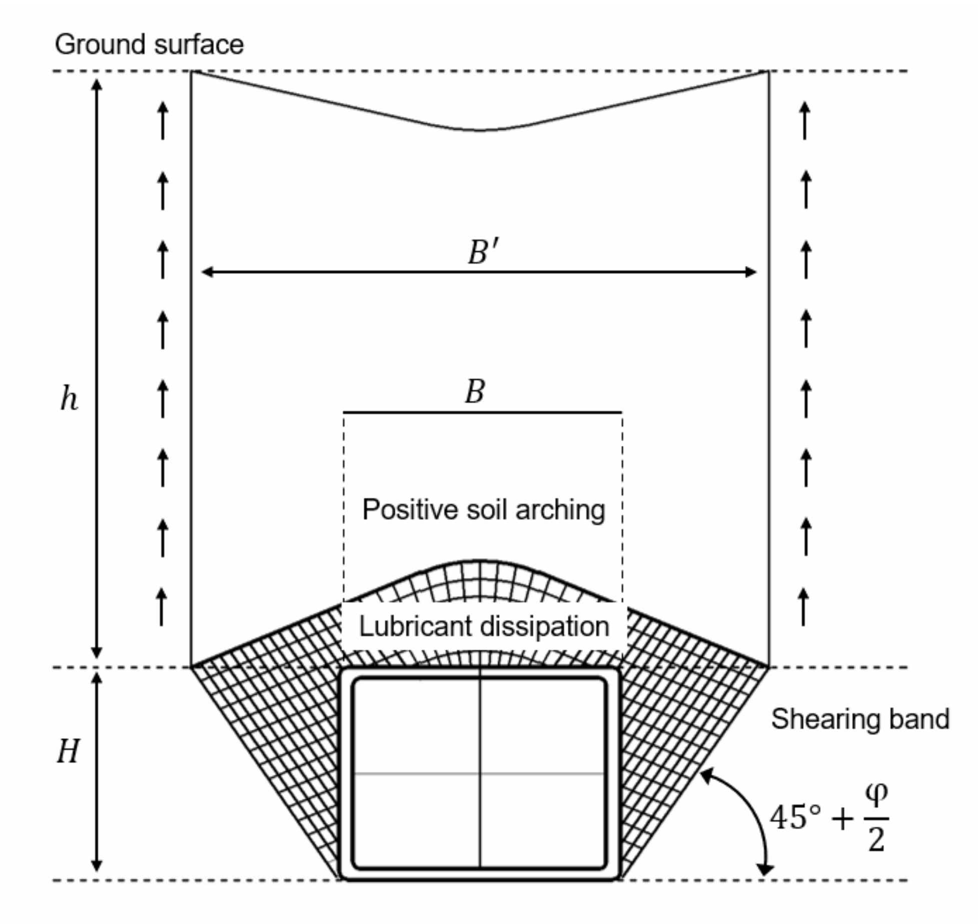

Fig. 15 Positive soil arching model.

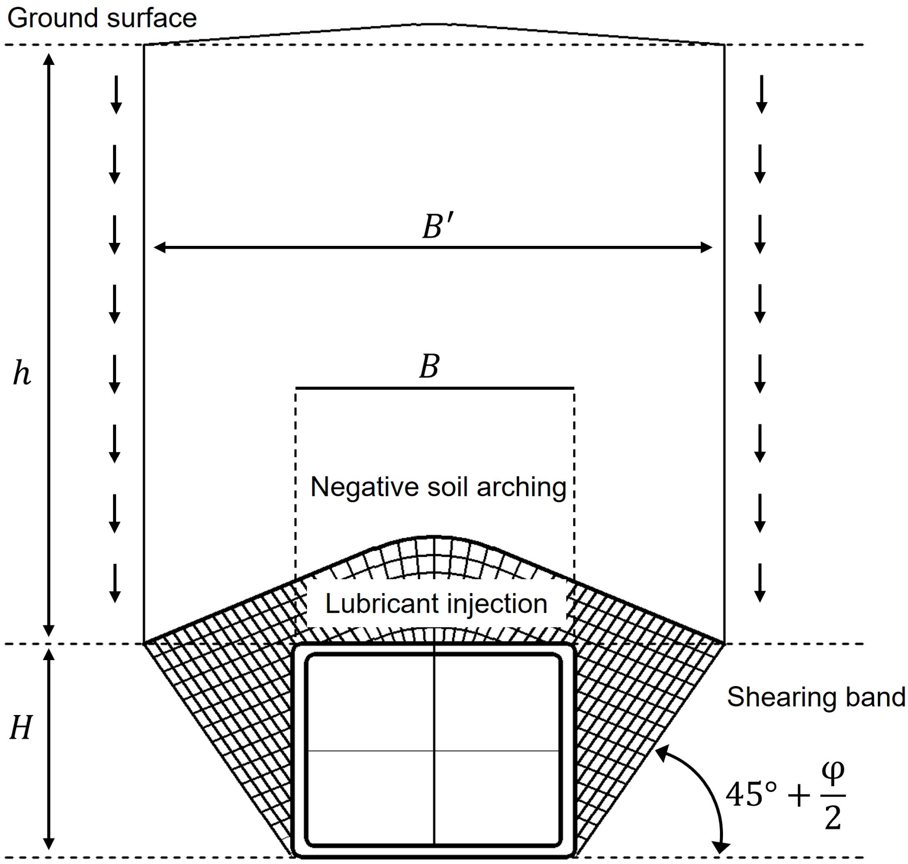

Fig. 16 Negative soil arching model.

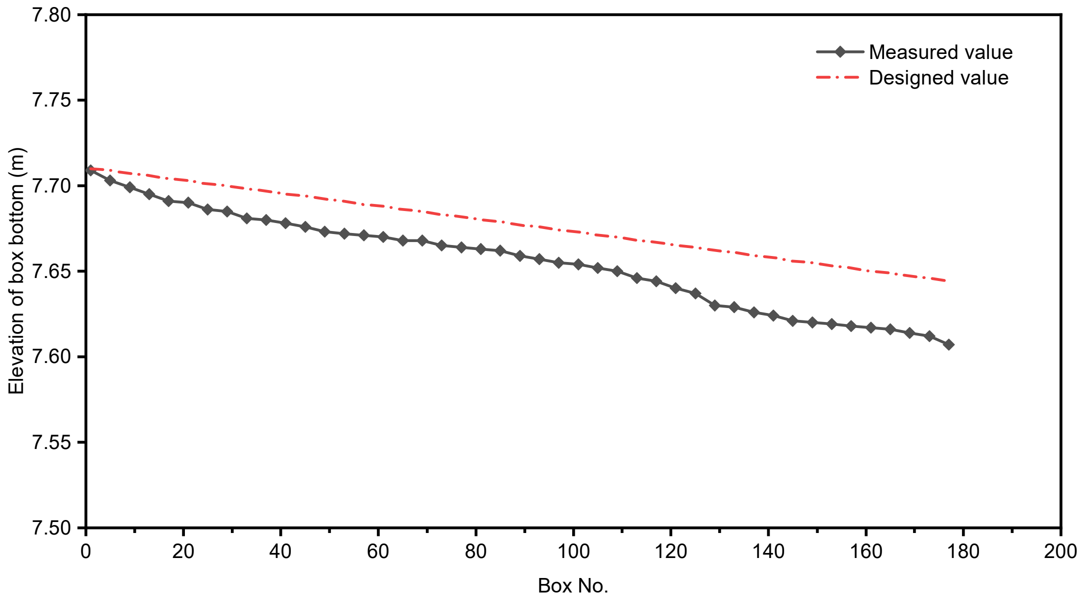

(a) vertical

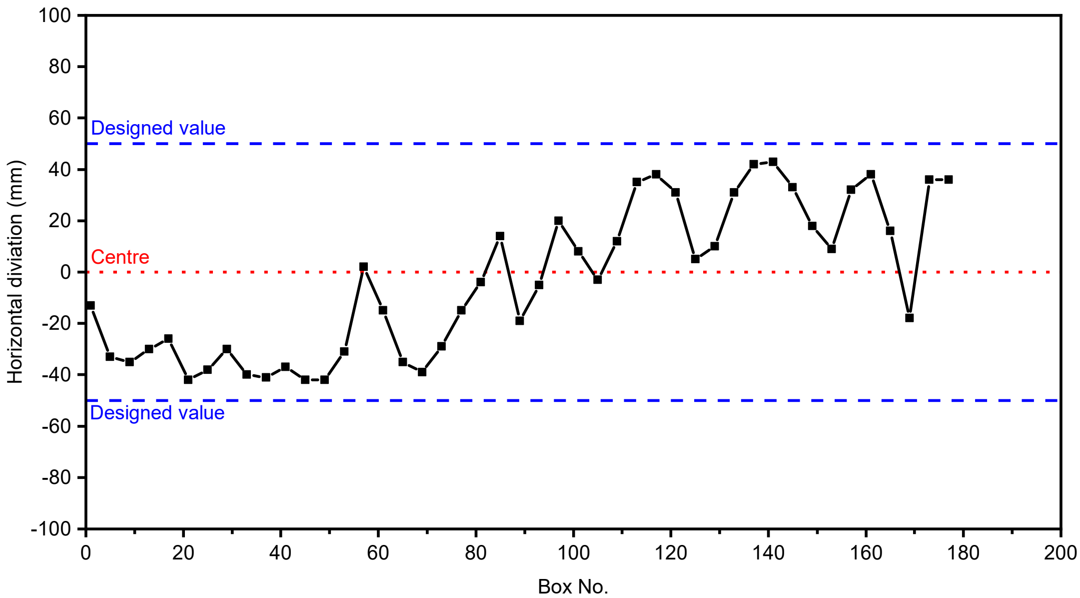

(b) horizontal

Fig. 17 deviation in alignment.

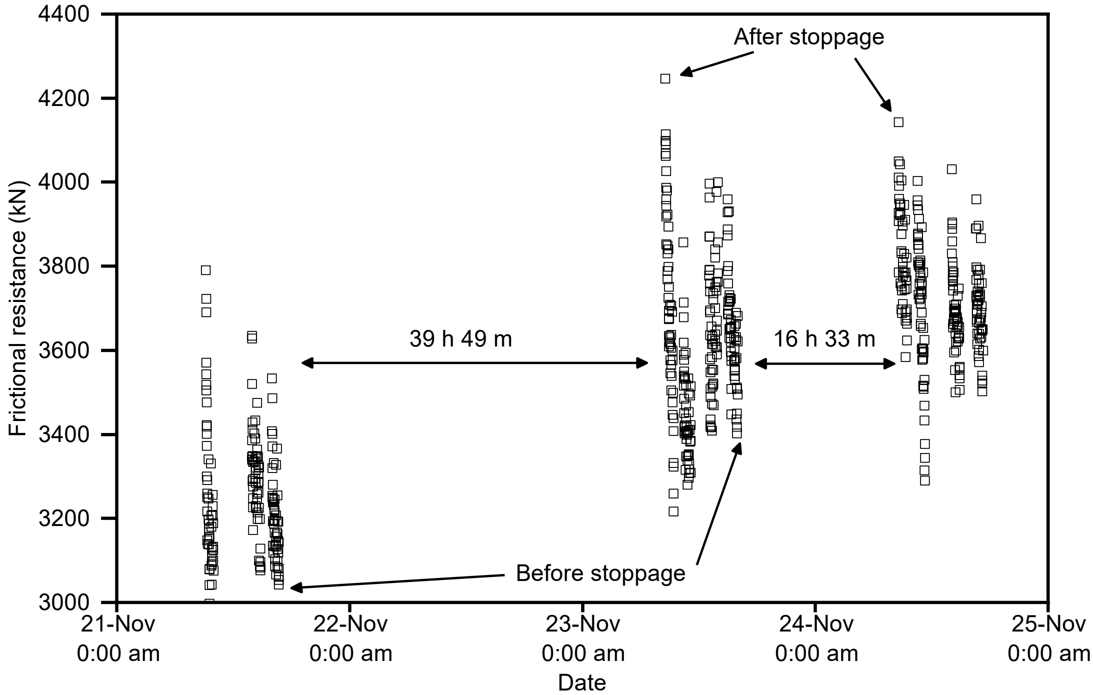

Fig. 18 Influence of stoppages on total frictional resistance.

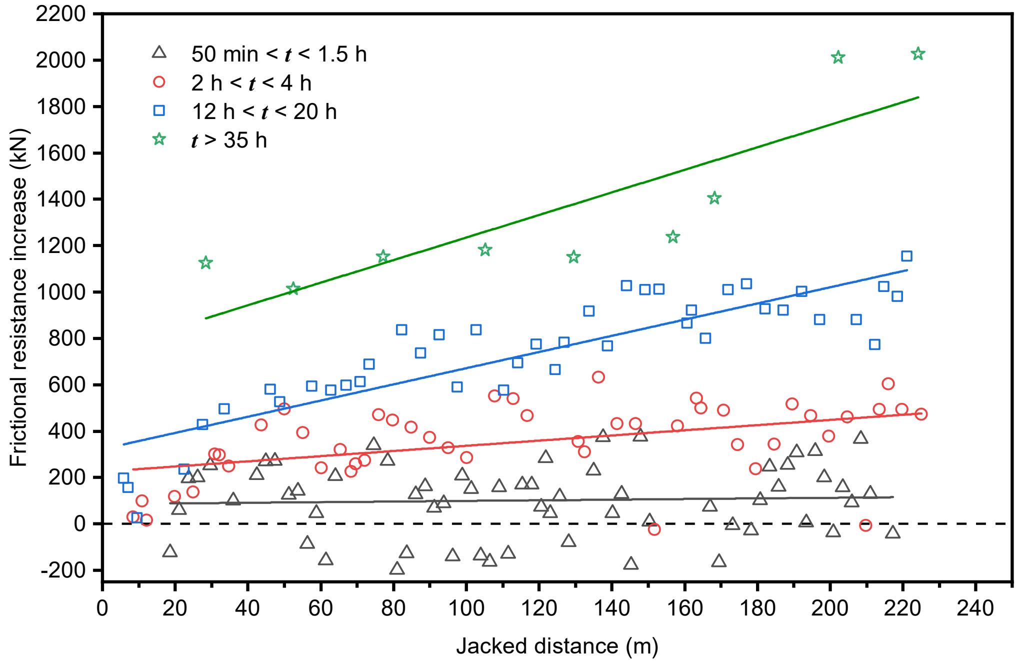

Fig. 19 Change in frictional resistance due to stoppage against jacked distance.

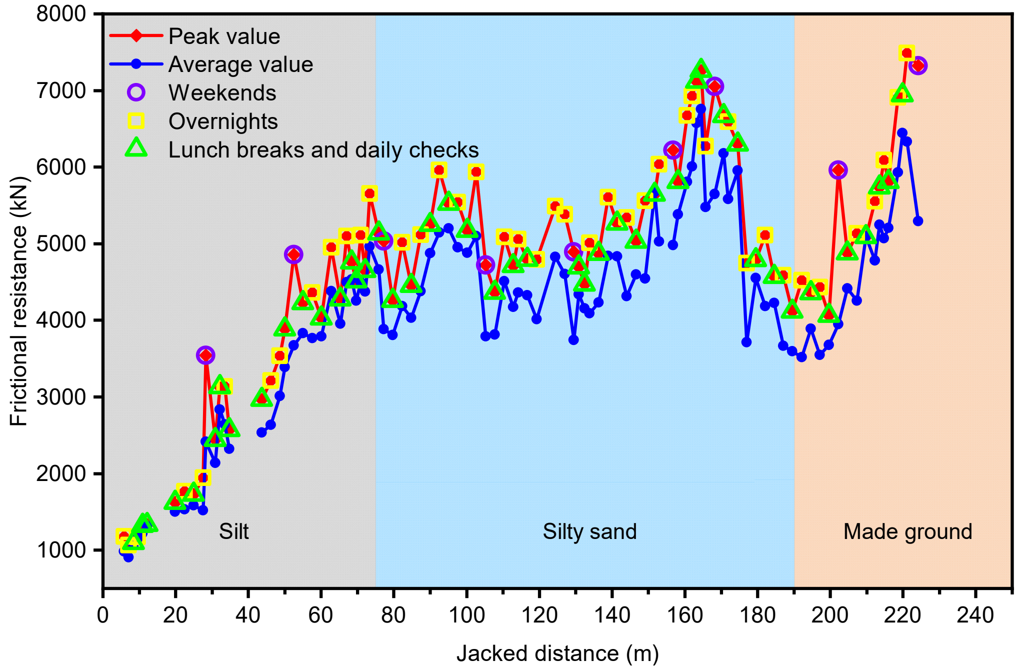

Fig. 20 The overall trend of frictional resistance increase.

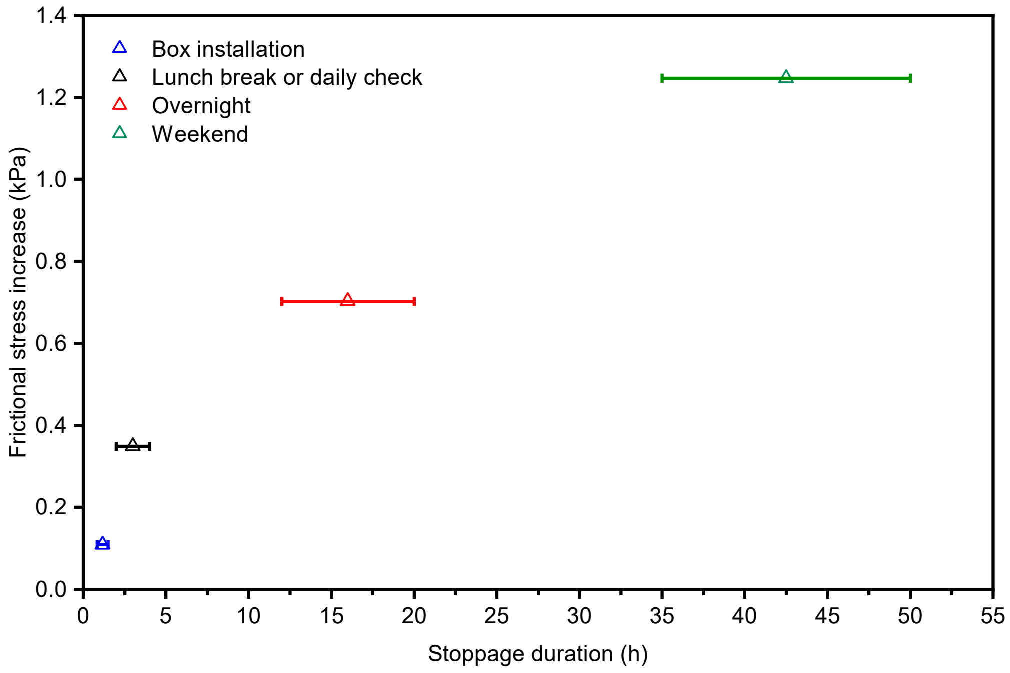

Fig. 21 Relationship between skin frictional stress increase and stoppage duration.

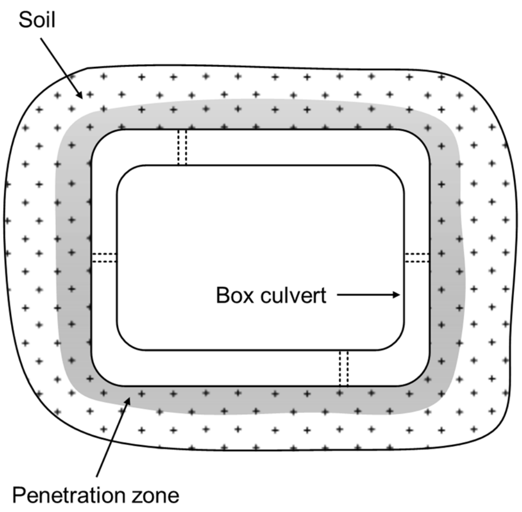

(a) Full box-soil interaction

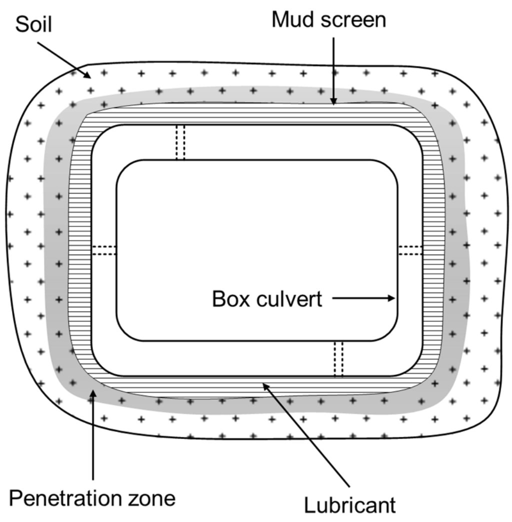

(b) Full box-lubricant interaction

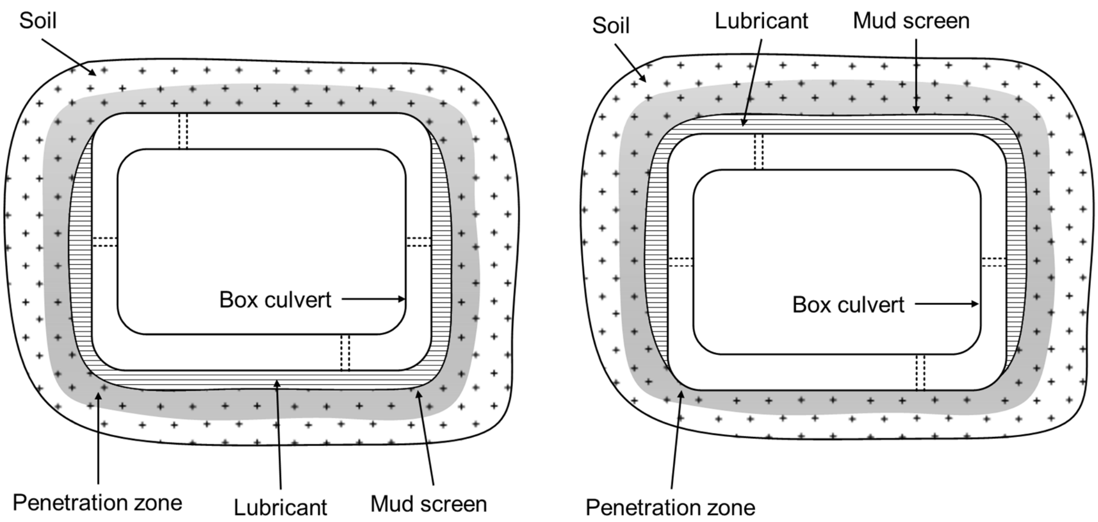

(c) One-side box-soil interaction

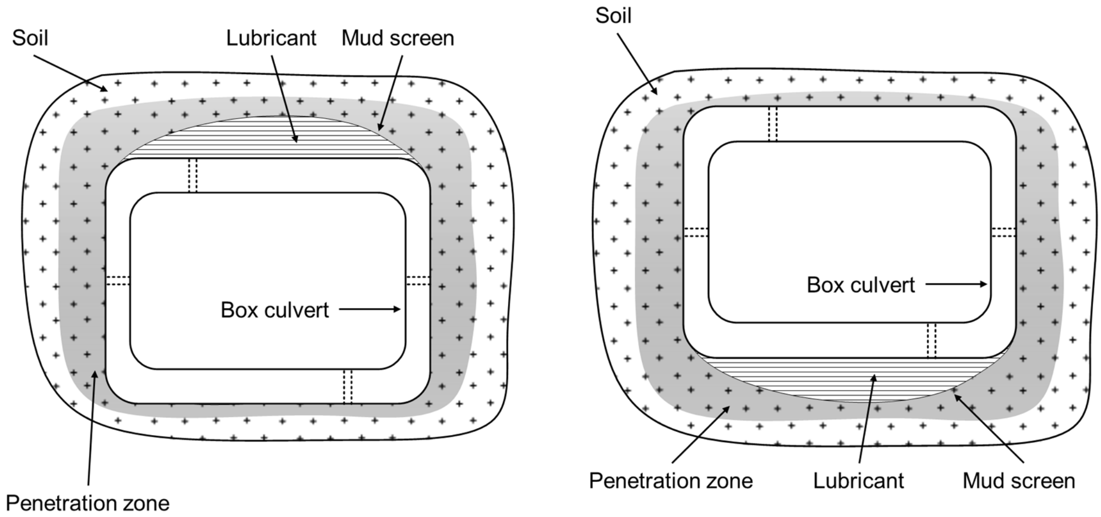

(d) Two-side box-soil interaction

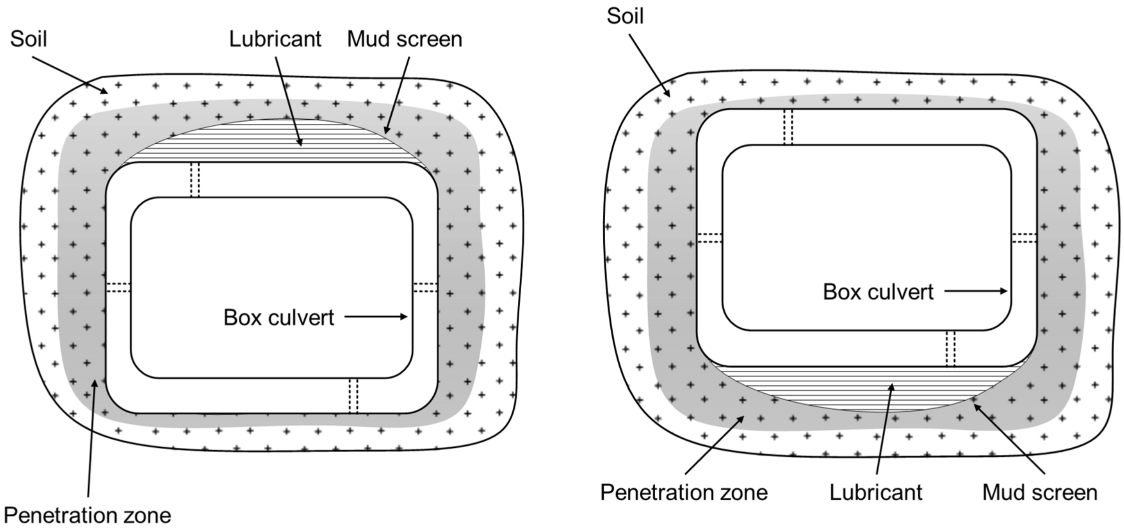

(e) Three-side box-soil interaction

Fig. 22 Five different contact status adapted from (Wen et al., 2020).

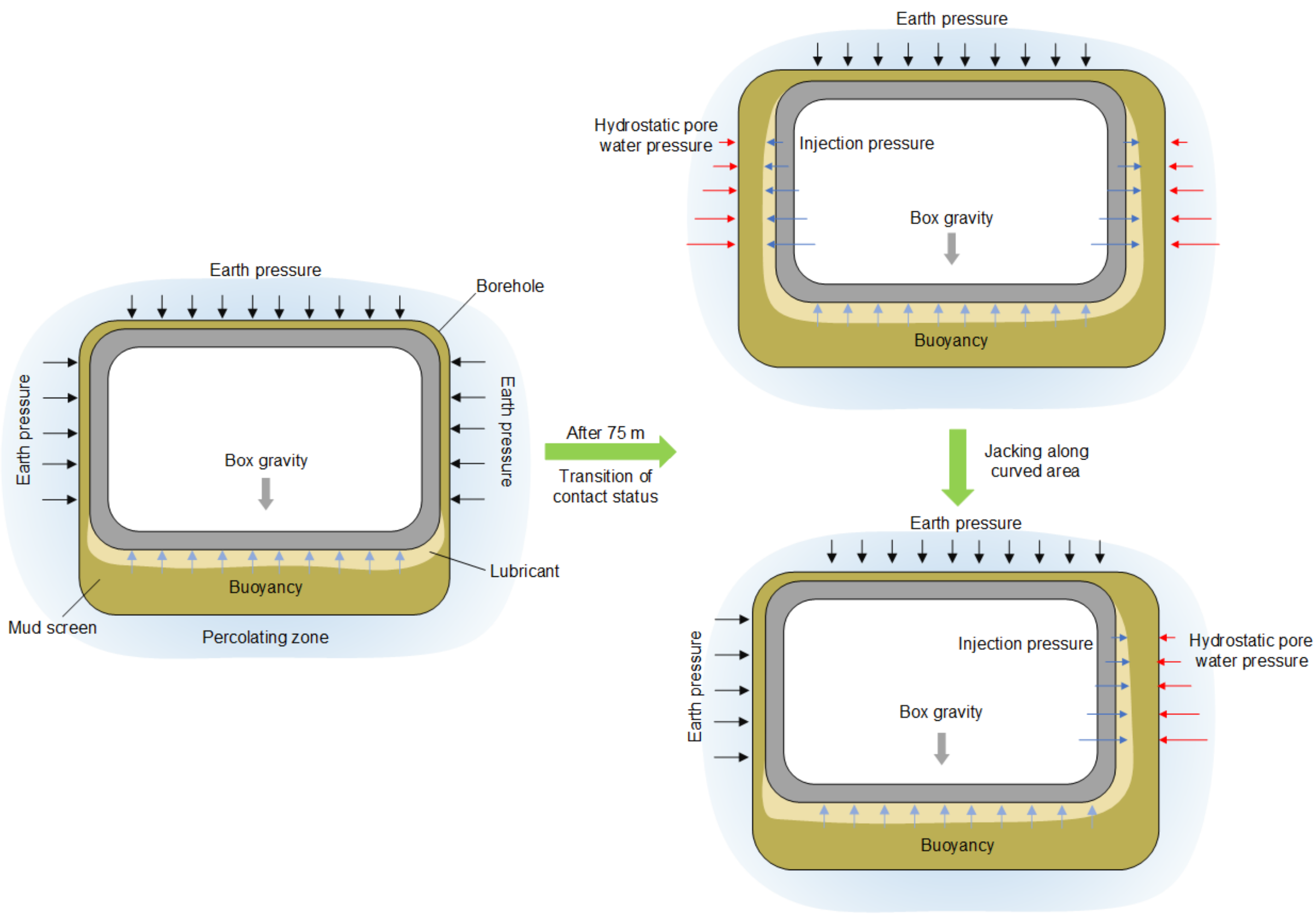

Fig. 23 Development of contact status during jacking process.

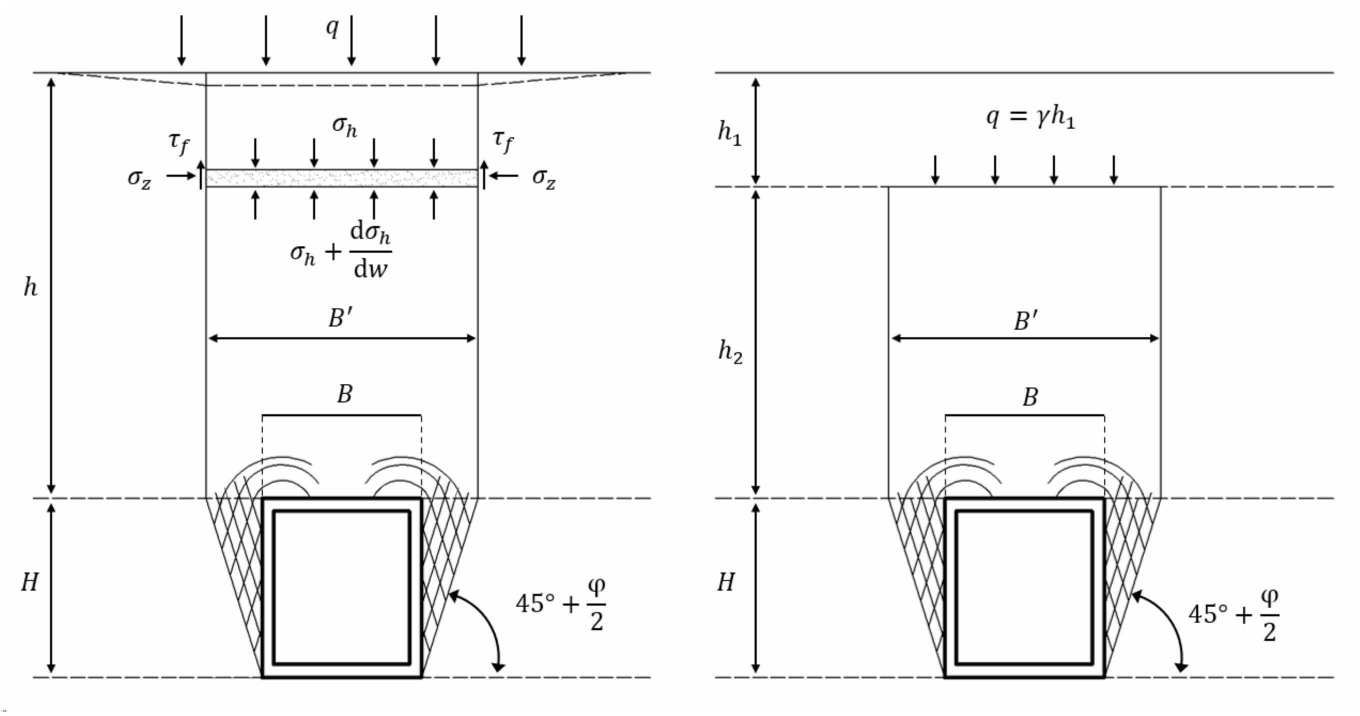

Fig. 24 Terzaghi silo model.

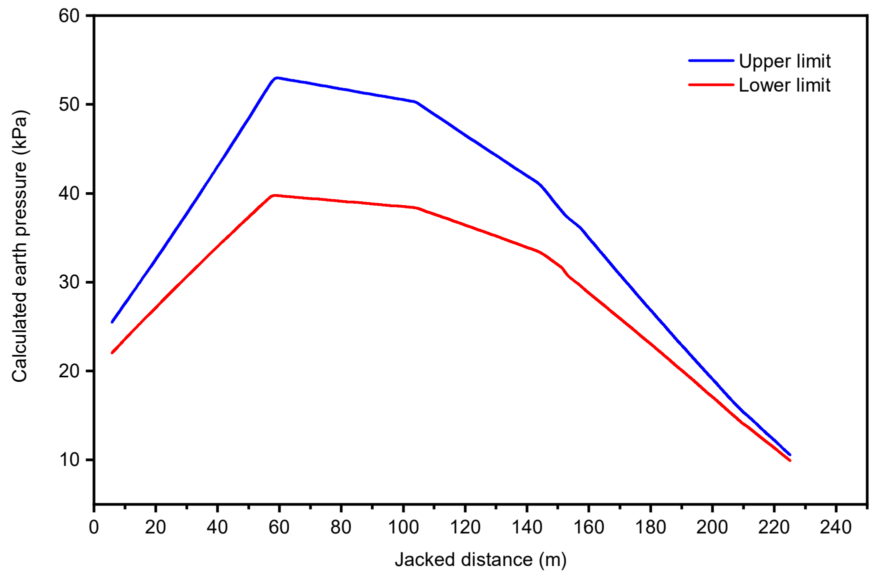

Fig. 25 The lower and upper limits of vertical earth pressure with jacking distance.

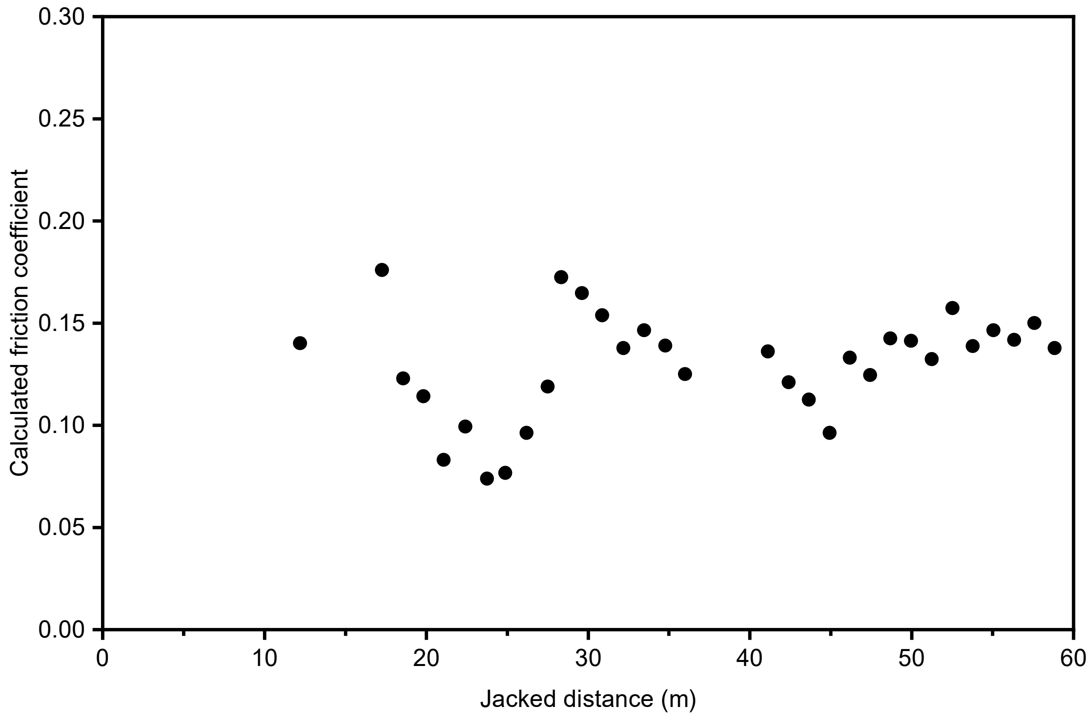

Fig. 26 Calculated friction coefficient.

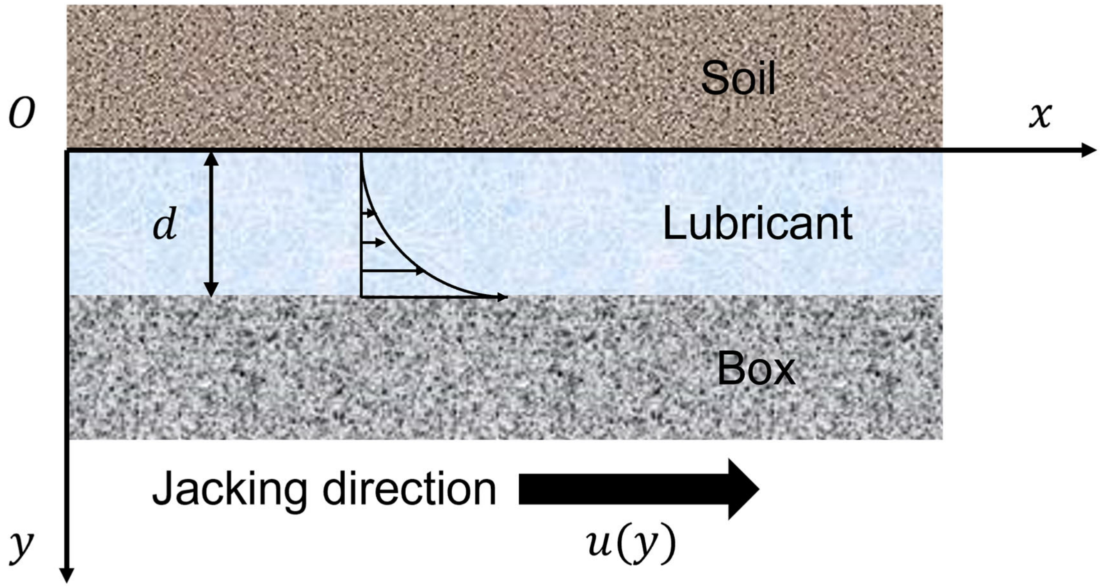

Fig. 27 Hydrodynamic parallel-plate model.

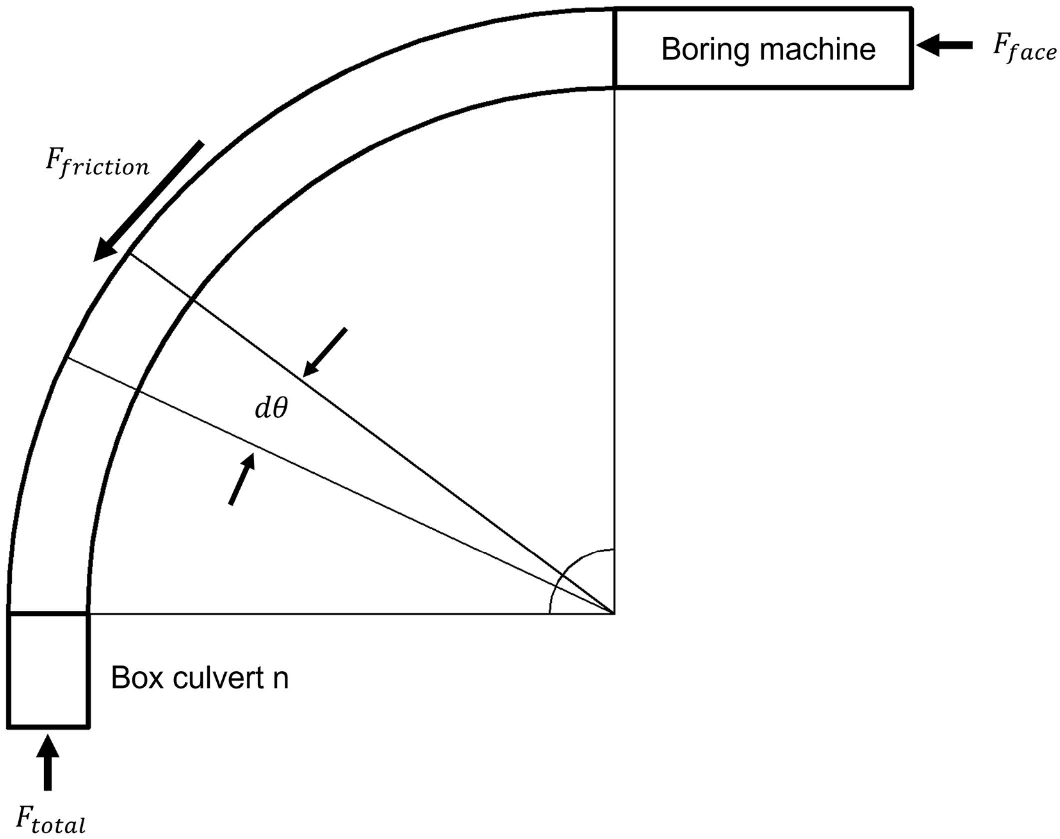

Fig. 28 Outside components of jacking force in a curved jacking area.

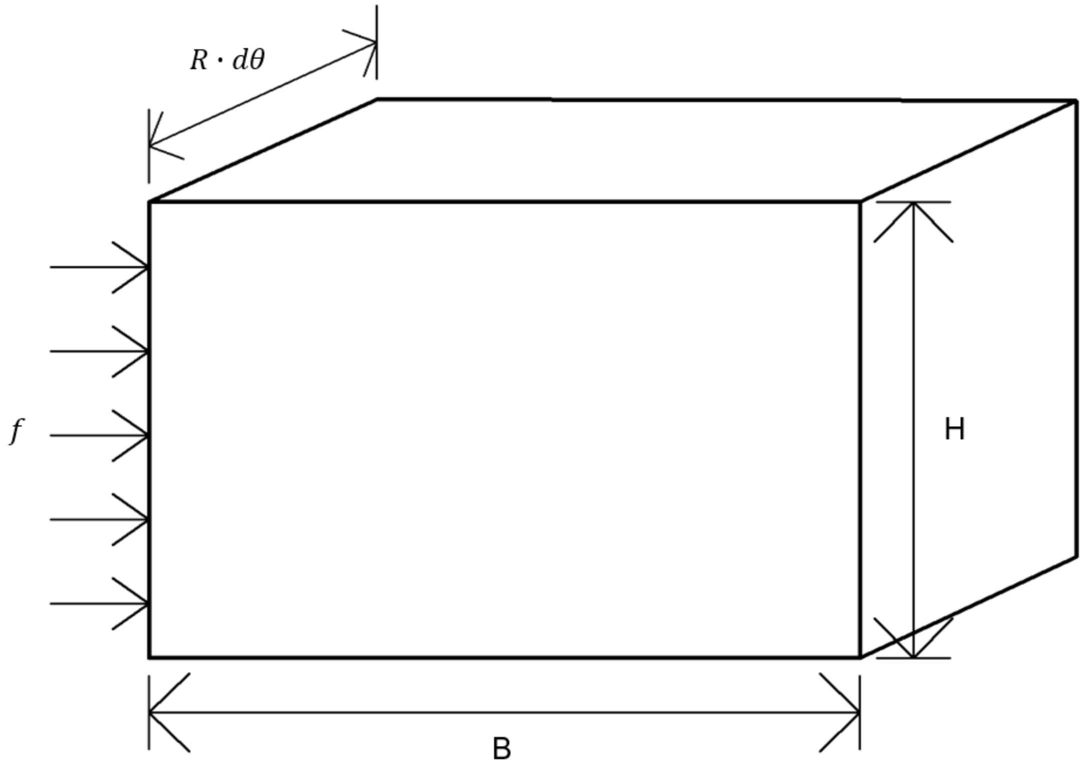

Fig. 29 Soil reaction against pushing box.

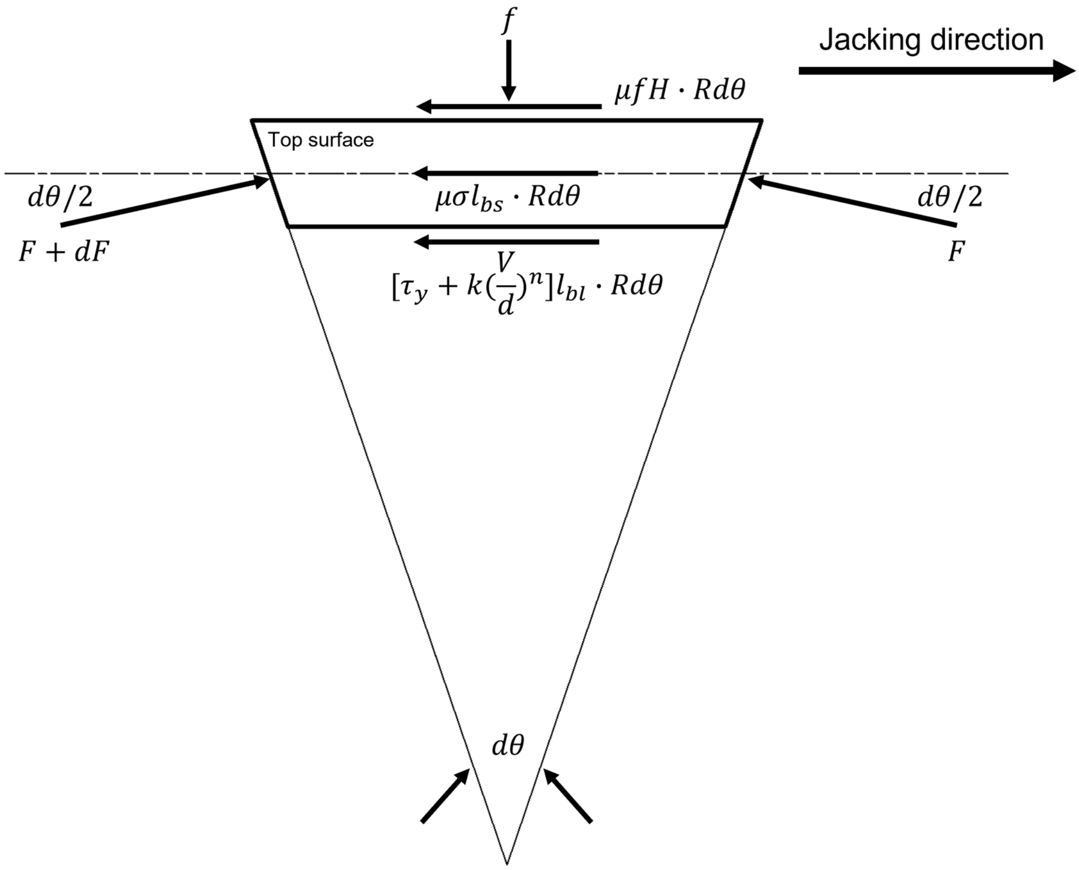

Fig. 30 Forces acting on a unit area.

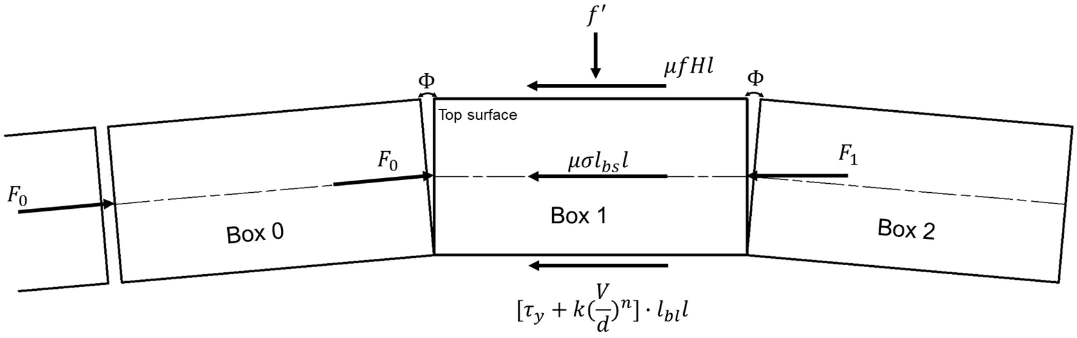

Fig. 31 Part of force analysis diagram for curved box jacking.

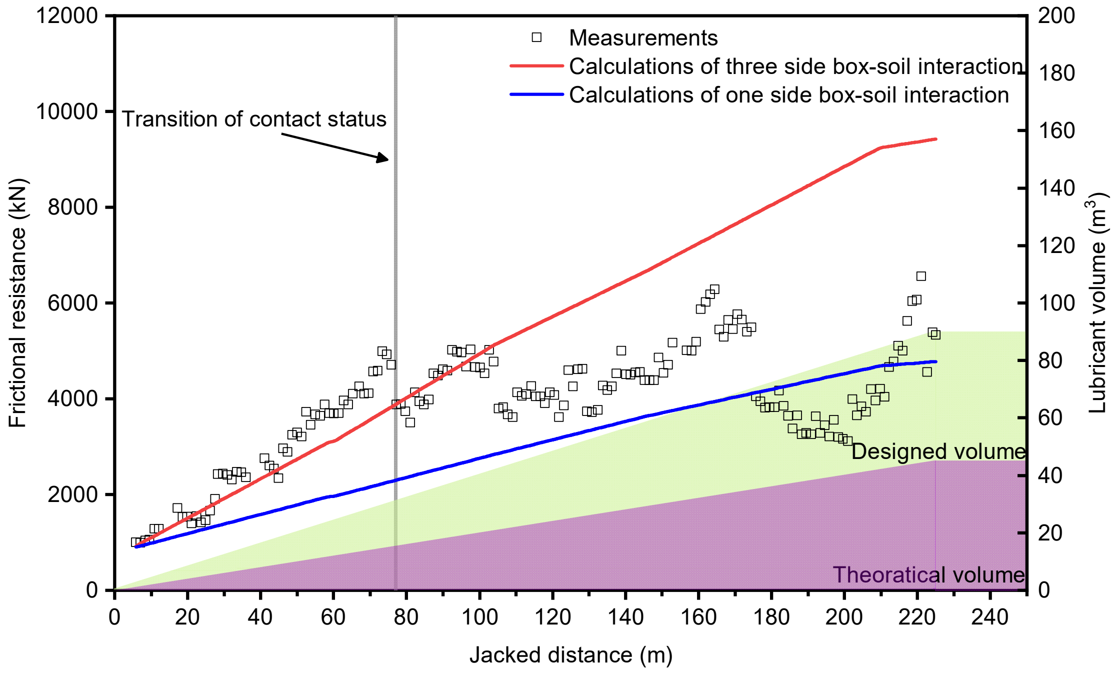

Fig. 32 Comparison between measured and calculated PBK frictional resistance.

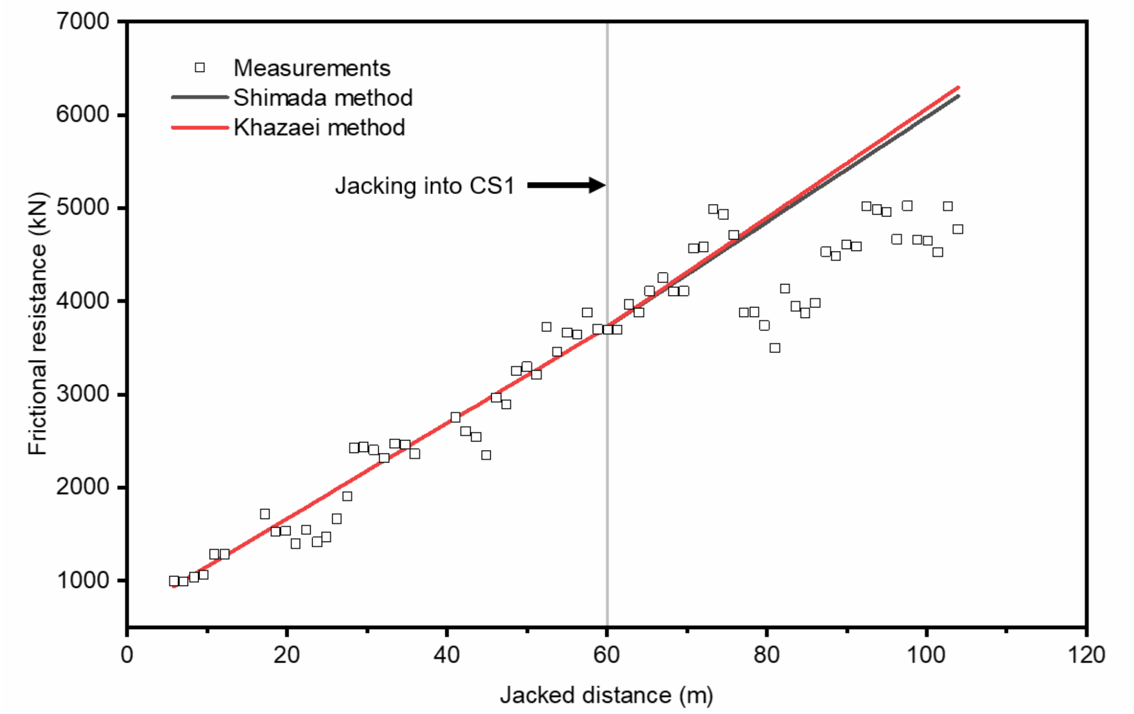

(a) Jacking into first curved section

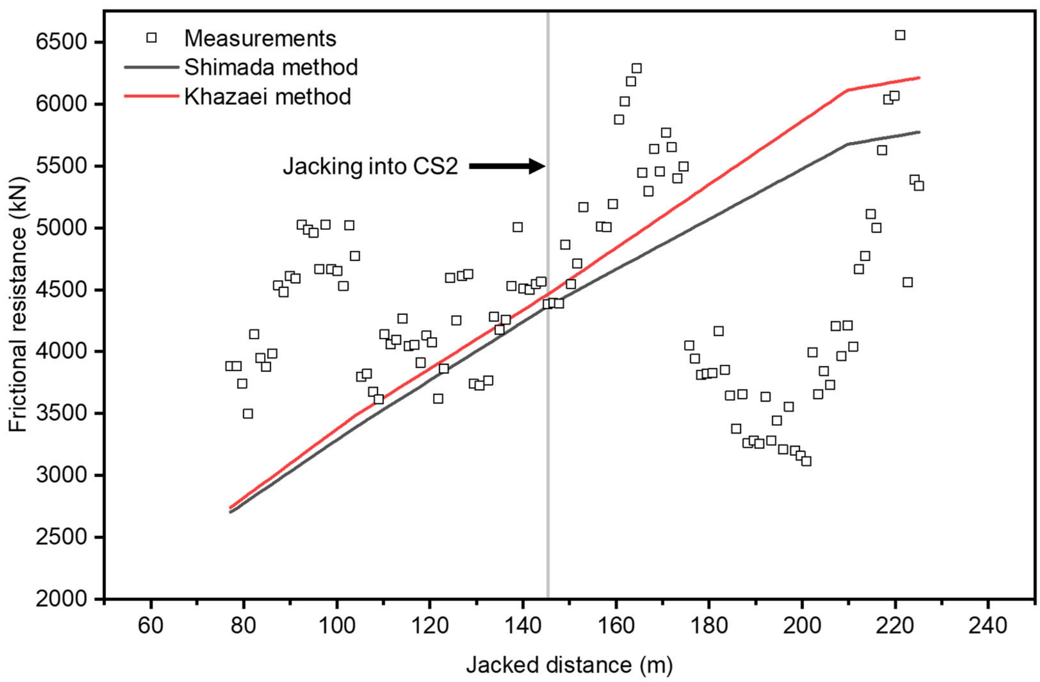

(b) Jacking into second curved section

Fig. 33 Comparison of calculated frictional resistance using Shimada and Khazaei methods for upper limit earth pressure in negative soil arching model.

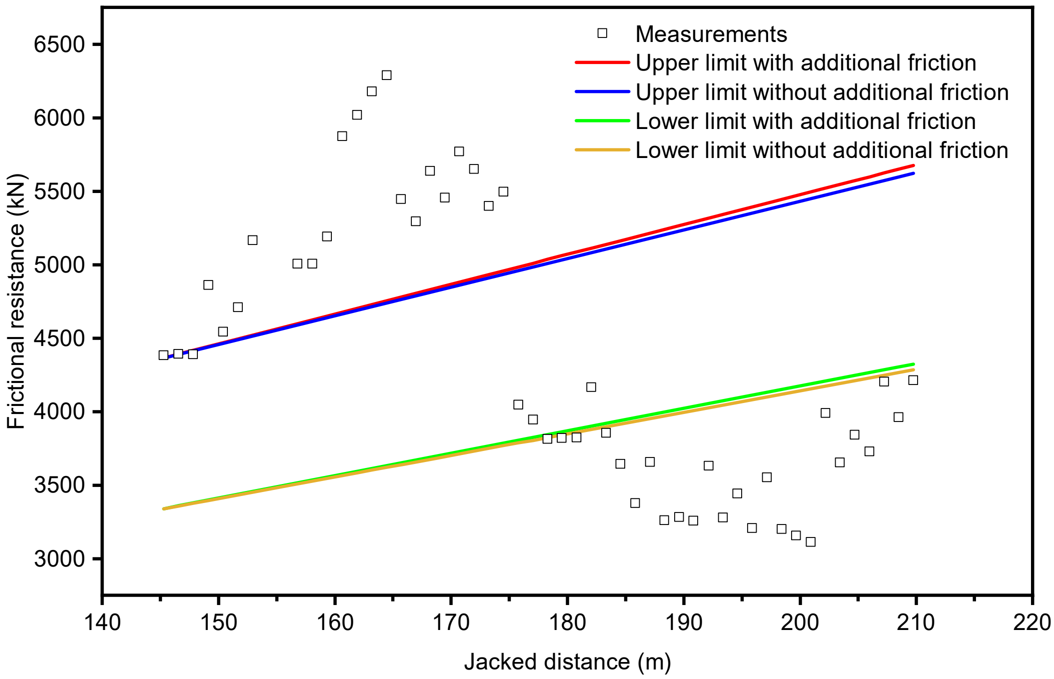

Fig. 34 Comparison of frictional resistance with and without additional frictional effects in the CS2 section.

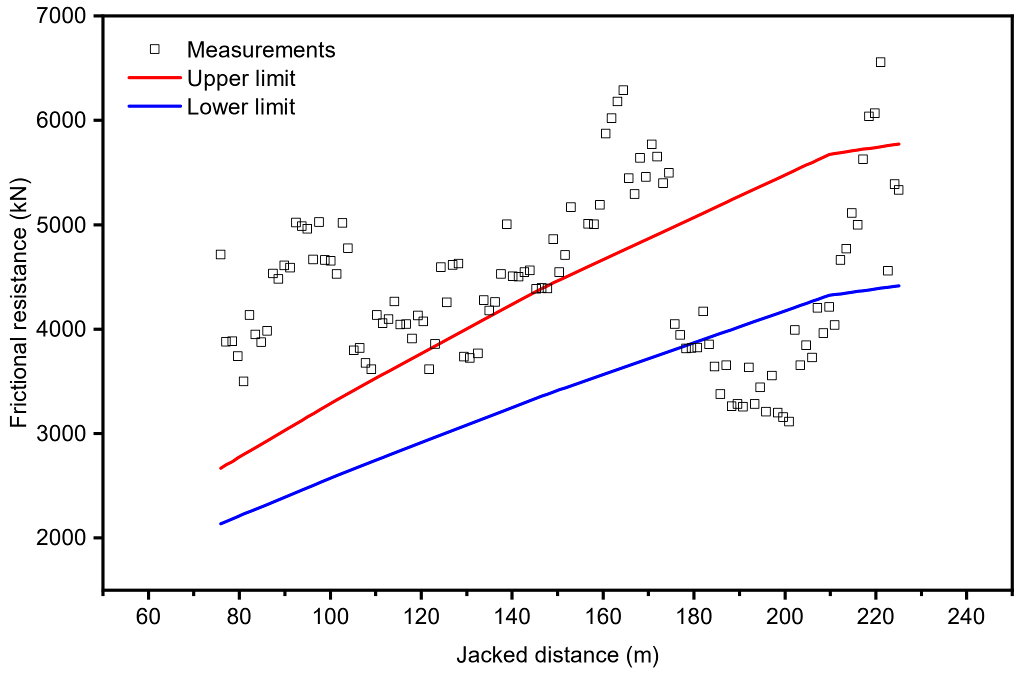

Fig. 35 Comparison between measured and calculated frictional resistance by revised SHIMADA method after 75 m.